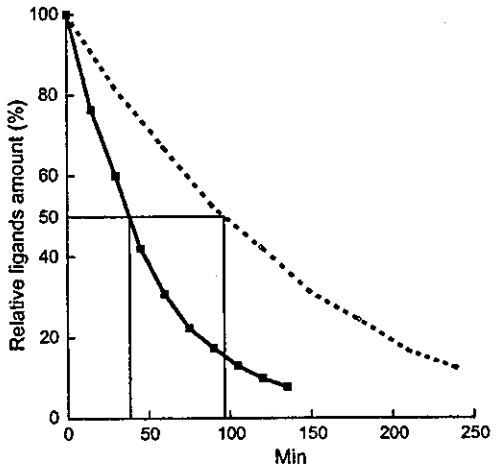

Figure 5. The half-life curves of ND (—) and NNC (···) in 100 mM sodium cacodylate buffer (pH 7.0) at 80 °C. *Y*-Axis represents the relative amount of ligands remained after incubation.

NNC is about 100 min. These results showed that the ligand NNC is much more thermally stable than ND.

The stabilities of the ligands in alkaline conditions were also examined incubating at room temperature in 50 mM sodium hydroxide (Fig. 6). Under the alkaline conditions, only 29% of ND remained after 2 h incubation, whereas 86% of NNC still remained under the same conditions. After incubation for 4 h, the amount of ND and NNC remaining was 7% and 79%, respectively. It is very clear that NNC is much more stable than ND in an alkaline solution.

Having confirmed the improved stability of NNC under the thermal and alkaline conditions, we then looked at

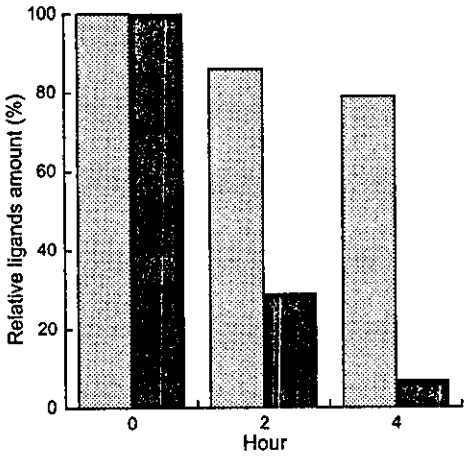

Figure 6. The amount of ND (solid bar) and NNC (shaded bar) (100 μM) remaining after incubation in 50 mM sodium hydroxide and 100 mM sodium chloride at room temperature. The amount was obtained by HPLC relative to the dT added as an internal standard. *Y*-Axis represents the relative amount of ligands remaining after incubation.

Table 1. ΔT_m of mismatch-containing duplexes in the presence ligands[a]

X–*Y*	T_m	ΔT_m[b]	
		NNC	ND
A–A	17.8 (1.4)	1.5 (0.2)	−0.8 (1.1)
A–C	16.1 (0.8)	4.1 (0.2)	2.1 (0.2)
C–C	18.2 (0.2)	6.1 (0.3)	6.7 (0.6)
G–A	25.7 (0.2)	7.0 (0.2)	8.6 (1.3)
G–G	25.6 (1.3)	29.1 (0.2)	23.7 (1.2)
G–T	28.3 (0.2)	1.2 (0.8)	10.2 (1.3)
T–C	18.6 (0.2)	3.7 (0.3)	5.5 (0.7)
T–T	25.1 (0.2)	0.7 (0.7)	0.6 (1.2)
A–T	34.3 (0.3)	0.0 (0.3)	−1.5 (0.3)
G–C	40.3 (0.0)	−2.0 (0.4)	2.0 (0.9)

[a] The UV-melting curve was measured for a duplex of d(CTA AC*X* GAA TG)/d(CAT TC*Y* GTT AG) at a total base concentration of 100 μM in a 10 mM sodium cacodylate buffer (pH 7.0) containing 0.1 M NaCl. A mismatch (*X*–*Y*) is produced in the middle of the duplex. Temperature was increased at a rate of 1 °C/min. All measurements were taken three times, and standard deviations are shown in the parentheses.

[b] ΔT_m is calculated as a difference of T_m in the presence and absence of drugs (100 μM), respectively.

the selective binding of NNC to the G–G mismatch. The assay was carried out by measuring the melting temperature (T_m) of 11-mer duplexes d(CTA AC*X* GAA TG)/d(CAT TC*Y* GTT AG) (where *X*, *Y* = A, G, T, or C) containing mismatches in the absence and presence of NNC (Table 1). T_m increase (ΔT_m) of the duplex containing a G–G mismatch was 23.7 °C in the presence of ND (100 μM). Under identical conditions, ΔT_m of 29.1 °C was recorded in the presence of NNC. The difference of ΔT_m ($\Delta\Delta T_m$) between NNC and ND for the G–G mismatch was 5.4 °C, suggesting that the modification of the linker structure of ND to that of NNC has a positive effect for the thermodynamic stabilization of the G–G mismatch by NNC. This is most likely due to an expanded π-surface in a carbamate linkage and a release of the linker strain involved in the bound DNA–ND complex. The affinity of NNC to the G–G mismatch was calculated by the curve fitting of the UV-melting curve obtained in the absence and presence of NNC to the theoretical equation.[14] The K_a obtained for the assumed 1:1 binding between NNC to the G–G mismatch was $>10^7 M^{-1}$, that is larger than the K_a we reported for the ND binding to the G–G mismatch.

All of the data presented here showed that the ligand NNC is a better ligand than ND in terms of the affinity and selectivity to the G–G mismatch, and the thermal and alkaline stability. The use of NNC for the SPR sensor would enhance the sensitivity to the G–G mismatch by eliminating the unnecessary binding to DNA containing other mismatches. Furthermore, with a higher thermal and alkaline stability, NNC can be applied more expansively than ND.

References and notes

1. Lander, E. S. et al. *Nature* **2001**, *409*, 860–921.
2. Venter, C. J. et al. *Science* **2001**, *291*, 1304–1351.

3. http://www.ncbi.nlm.nih.gov/SNP/.
4. Schafer, A. J.; Hawkins, J. R. *Nat. Biotechnol.* **1998**, *16*, 33–39.
5. Collins, F. S.; Guyer, M. S.; Chakravarti, A. *Science* **1997**, *278*, 1580–1581.
6. SyvaÈnen, A. C. *Nature Rev. Genet.* **2001**, *2*, 930–942.
7. Kwok, P. Y. *Annu. Rev. Genom. Hum. Genet.* **2001**, *2*, 235–258.
8. Nakatani, K.; Sando, S.; Saito, I. *Nat. Biotechnol.* **2001**, *19*, 51–55.
9. Nice, E. C.; Catimel, B. *Bioessays* **1999**, *21*, 339–352.
10. Fivash, M.; Towler, E. M.; Fisher, R. *Curr. Opin. Biotechnol.* **1998**, *9*, 97–101.
11. Nakatani, K.; Sando, S.; Kumasawa, H.; Kikuchi, J.; Saito, I. *J. Am. Chem. Soc.* **2001**, *123*, 12650–12657.
12. Ghosh, A. K.; Duong, T. T.; McKee, S. P.; Thompson, W. J. *Tetrahedron Lett.* **1992**, *33*, 2781–2784.
13. The data of the hydrochloride salt of NNC: ^{1}H NMR (CD_3OD, 400 MHz): $\delta = 8.15$ (m, 6H), 7.35 (d, 2H, $J = 8.4$ Hz), 4.34 (t, 4H, $J = 6.0$ Hz), 3.15 (t, 4H, $J = 7.2$ Hz), 2.71 (s, 6H), 2.11 (br s, 4H). ^{13}C NMR (CD_3OD, 400 MHz): $\delta = 163.0$, 154.5, 154.3, 154.0, 139.1, 137.6, 121.4, 118.2, 113.1, 62.7, 45.4, 26.5, 23.8. HR-FABMS calcd for $C_{26}H_{30}N_7O_6$ [$(M+H)^+$], 504.2359. Found: 504.2361.
14. Nakatani, K.; Horie, S.; Murase, T.; Hagihara, S.; Saito, I. *Bioorg. Med. Chem.* **2003**, *11*, 2347–2353.

Nucleic Acids Symposium Series No. 48 123-124

Separation of mismatched DNA by using the affinity column immobilizing mismatch-binding ligands

Yuki Goto[1], Akio Kobori[2], Hitoshi Suda[1] and Kazuhiko Nakatani[1,2]
[1]Department of Synthetic Chemistry and Biological Chemistry, Faculty of Engineering, Kyoto University, Kyoto 615-8510, Japan and [2]PRESTO, Japan Science and Technology Agency (JST), Kawaguchi City, Saitama 332-0012, Japan

ABSTRACT

Mismatch-binding ligands (MBL), ND and NA, bind to DNA containing mismatch base pairs. These MBLs were immobilized to NHS-activated affinity column via amine linker. Affinity chromatographic analyses of mismatched DNAs by using the ND-immobilized column showed clear separation of G-G and G-A from other mismatched DNAs. The results of the NA-immobilized column also showed good separation of A-A, G-A, G-G, A-C from other mismatched DNAs. The order of mobility of mismatched duplexes on MBL-immobilized column was in good agreement with that of the binding affinity in a solution phase obtained by the melting temperature measurements.

INTRODUCTION

High-throughput SNPs typing methods are expected to be needed for realizing personalized medicine. One of methods for SNPs typing is heteroduplex analyses which detect heteroduplex DNA, containing a single mismatched site, generated by hybridization of two sets of duplex DNAs that differ from each other by a single nucleotide. Conventional low-throughput methods for the detection of mismatched DNAs in heteroduplex analyses were enzymatic and chemical cleavage at the mismatched site, gel electrophoresis, and the binding of mismatch-binding proteins.

We have reported mismatch-binding ligands (MBL) that bind to specific mismatch base pairs in the DNA duplex.[1-3] We have immobilized MBLs on SPR sensors providing novel mismatch-detecting sensors for high-throughput heteroduplex analyses.[1-3]

We here report novel applications of MBLs in the separation of mismatched DNA with the MBL-immobilized affinity chromatography. This technique will provide high-throughput and inexpensive method of SNPs typing.

RESULTS AND DISCUSSION

We have reported two MBLs, naphthyridine dimer (**ND**) and naphthyridine-azaquinolone (**NA**).

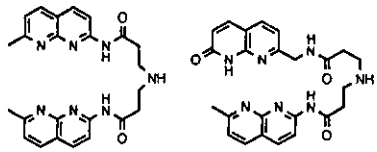

ND **NA**

ND strongly binds to G-G mismatch, whereas **NA** binds to A-A and G-A mismatches.

ND and **NA** were first attached to the short amine linker, and then immobilized on HiTrap NHS-activated HP Column (Amersham Biosciences). These MBL-immobilized columns were connected to ÄKTAexplorer system (Amersham Biosciences). The performance of the MBL-immobilized columns were examined by the analyses of hairpin DNAs, 5'-d(CTA ACX GAA TGT TTT CAT TCY GTT AG)-3', containing mismatched base pairs (***Figure 1***). The DNAs were eluted with a solvent mixture of running buffer [100 mM NaCl, 10 mM Na phosphate pH = 7.0], 0-10% elution buffer [100 mM NaCl, 50 mM NaOH]/3-4 min, 10-35%/4-14 min, and 35-50%/14-16 min at a flow rate 1.0 mL/min. Retention time (t_R) and half width ($W_{1/2}$) of the peak of each mismatched DNA was summarized in ***Figure 2***. G-G and G-A mismatched DNAs were strongly retained on **ND**-immobilized column and were eluted with flowing the elution buffer. Other mismatched and full matched DNAs were eluted from the column with the running buffer. t_R of C-C, G-T, and T-C mismatched DNAs (1.32-1.84 min) obviously differed from that of full matched DNAs (1.15-1.17 min), and $W_{1/2}$ of C-C, G-T, and T-C mismatched DNAs (0.44-0.87 min) were wider than that of full matched DNAs (0.35 min).

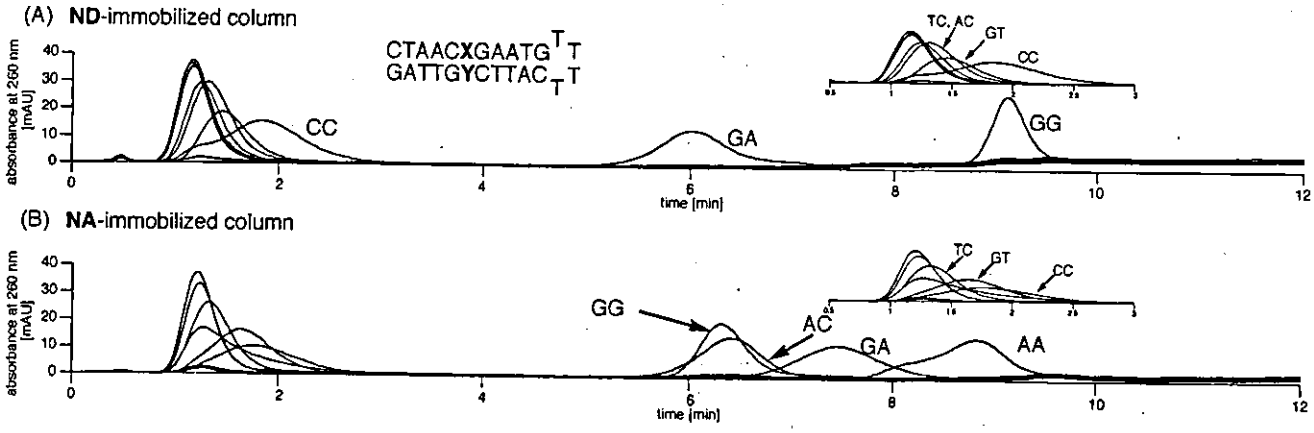

Figure 1. The affinity chromatography analyses of hairpin DNAs containing mismatched base pairs by using (A) ND-immobilized column and (B) NA-immobilized column. Inset: for clarity, the range of time from 0.5 to 3.0 was shown.

	ND			NA		
sequence	t_R (min)	$W_{1/2}$ (min)	ΔT_m (°C)	t_R (min)	$W_{1/2}$ (min)	ΔT_m (°C)
GG	9.12	0.37	24.0	6.33	0.52	6.8
GA	6.03	0.69	11.7	7.46	0.89	12.1
GT	1.45	0.51	9.9	1.78	0.89	1.4
GC	1.17	0.35	2.6	1.22	0.35	0.9
AA	1.17	0.36	2.4	8.83	0.85	31.8
AT	1.15	0.35	-1.3	1.28	0.59	0.4
AC	1.25	0.39	4.8	6.42	0.69	6.7
TT	1.17	0.36	-0.8	1.24	0.35	0.4
TC	1.32	0.44	2.7	1.33	0.44	2.3
CC	1.84	0.87	5.5	1.64	0.69	4.2

Figure 2. The retention time (t_R) and half width ($W_{1/2}$) of the peak of each mismatched DNA in the affinity chromatograph were shown. ΔT_m values of 11-mer duplex with MBLs were also shown.

These observations suggested that these mismatched DNAs were separated by the weak interactions between DNAs and **ND** surface on the solid support. In the case of **NA** column, A-A, G-A, G-G, and A-C mismatched DNAs were retained on **NA** surface, whereas other mismatches were eluted with running buffer. C-C, G-T, and T-C mismatched DNAs were not retained strongly, but their t_R (1.33-1.78 min) were larger than that of full matched DNA (1.22-1.28 min). These results of the affinity chromatography indicated that the MBL-immobilized columns are useful to separate not only mismatched DNAs strongly binding but also those weakly binding to the surface.

Basic information regarding MBL-mismatch binding was obtained by measuring the difference in melting temperature (ΔT_m) of 11-mer duplex, 5'-d(CTA ACX GAA TG)-3'/3'-d(GAT TGY CTT AC)-5', in the absence and presence of MBLs. **ND** bound not only to G-G mismatched duplex as reported, but weakly to G-A, G-T, and C-C mismatched duplexes. On the other hand, **NA** bound not only to A-A and G-A mismatched duplexes but also G-G, A-C, and C-C mismatched duplexes with decreased efficiency. The order of mobility of mismatched duplex on MBL-immobilized column was in good agreement with that of the binding affinity in a solution phase obtained by T_m measurements.

The results described here demonstrated the potential of MBLs and MBL-immobilized surfaces for the affinity separation of single mismatched duplexes. The advantage of the use of the MBL-immobilized surfaces is the redundancy of any DNA labeling, which significantly reduces the cost and simplify the assay procedure of SNPs typing.

REFERENCES

1. Nakatani, K., Sando, S. and Saito, I. (2001) *Nat. Biotechnol.*, **19**, 51-55.
2. Hagihara, S., Kumasawa, H., Goto, Y., Hayashi, G., Kobori, A., Saito, I. and Nakatani, K. (2004) *Nucleic Acids Res.*, **32**, 278-286.
3. Kobori, A., Horie, S., Suda, H., Saito, I. and Nakatani, K. (2004) *J. Am. Chem. Soc*, **126**, 557-562

Nucleic Acids Symposium Series No. 48 129-130

SPR fingerprinting of mismatched base pair

Akio Kobori[1], Tao Peng[1], Gosuke Hayashi[2] and Kazuhiko Nakatani[1,2]
[1]PRESTO, Japan Science and Technology Agency and [2]Department of Synthetic Chemistry and Biological Chemistry, Faculty of Engineering, Kyoto University, Kyoto 615-8510, Japan

ABSTRACT

Discrimination of mismatched base pairs having various flanking sequence from normal Watson-crick base pairs were examined using SPR sensor surface where mismatch binding ligand (MBL) were immobilized. CC, CT, and TT mismatched base pair are distinguishable from wild type DNA by means of diaminonaphthyridine dimer (damND) immobilized sensor surface. By comparing the component ratio of responses obtained by MLB immobilized sensors, distinct differences could be observed between mismatched base pairs having almost the same total SPR response.

INTRODUCTION

Surface Plasmon Resonance (SPR) is an effective tool for directly visualizing the ligand-substrate interactions occurring on the sensor surface. We have studied the mismatch binding ligands (MBL) that selectively and strongly bind to the mismatched base pairs, and developed the SPR sensor surface where MBL are immobilized to detect the mismatched base pairs. Naphthyridine dimer (ND) that contains two naphthyridine chromophores and linker selectively binds to G-G mismatched base pair.[1] Naphthyridine-azaquinolone (NA) and aminonaphthyridine (amND) dimer bind to G-A and C-C mismatched base pairs, respectively.[2,3] Mismatch-detecting sensors were synthesized by immobilizing these ligands on gold surface. To distinguish all eight base mismatches from Watson-Crick base pairs, we have investigated the fingerprinting of base mismatches by these MBL. In addition to three MBL, a new MBL diaminonaphthyridine dimer (damND) was used for the fingerprinting. We here report the fingerprinting of mismatched base pairs flanked by all possible sequences.

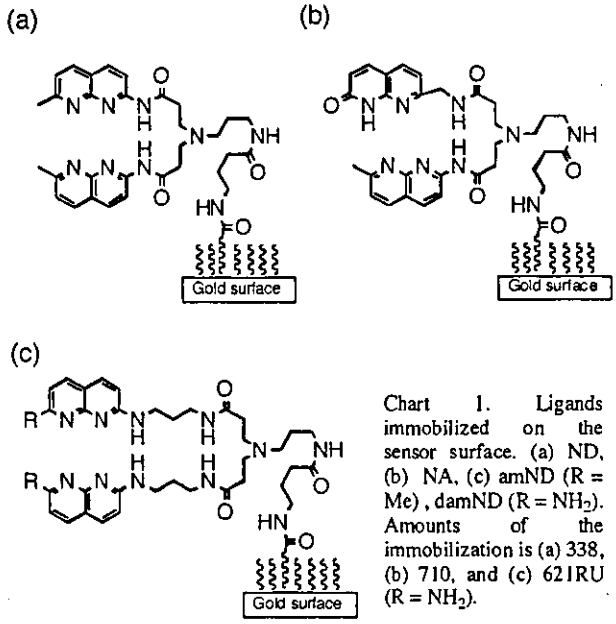

Chart 1. Ligands immobilized on the sensor surface. (a) ND, (b) NA, (c) amND (R = Me), damND (R = NH_2). Amounts of the immobilization is (a) 338, (b) 710, and (c) 621RU (R = NH_2).

RESULTS and DISCUSSION

Preparation of the ligand immobilized surface

MBL was immobilized on an activated carboxyl terminal attached to the dextran surface according to the procedure

recommended by Biacore. A 1 mM solution of MBL having a primary amino group at the linker termini in 10 mM of a borate buffer (pH = 9.2) was applied to the carboxylic acid of the CM5 sensor chip activated with *N*-hydroxysuccinimide and EDCI.

SPR fingerprinting of mismatched base pairs

The effect of the mismatched base pair with various flanking sequences on the binding to the ligand was examined using ND, NA, amND, and damND immobilized sensor surface. SPR analyses of mismatch-containing 27-mer 5'-d(GTT ACA GAA TCT N_1XN_2 AAG CCT AAT ACG)-3'/3'-d(CAA TGT TTC AGA N_3YN_4 TTC GGA TTA TGC)-5' were performed in HEPES buffer (pH 7.4) containing 500 mM NaCl. In addition to the GG and CC mismatches examined by ND and amND immobilized surface, the response at 180 sec after injection of DNA duplexes containing CT or TT mismatch were larger than 170 RU for all flanking sequences. These responses are more than 4 times larger than that for AT matched base pair (50 RU). Therefore, GG, CC, CT, and TT mismatched base pair are distinguishable from normal Watson-Crick base pair by single ND or damND immobilized sensor surface.

Fingerprinting of the remaining four mismatches, CA, GA, AA, and GT, which showed insufficient responses to each MBL-immobilized surface was carried out by taking a sum of responses obtained by damND, ND, and NA immobilized sensor surfaces at 180 sec. Typical examples of fingerprinting were shown for CCC/GAG (N_1XN_2/N_3YN_4), CGG/GAC, CCG/GAC, AGG/TTC, and CAG/GAC containing duplexes. (Figure 1) The sum of responses for the five mismatched base pairs was more than 200 RU and obviously distinguishable from the back ground noise. By comparing

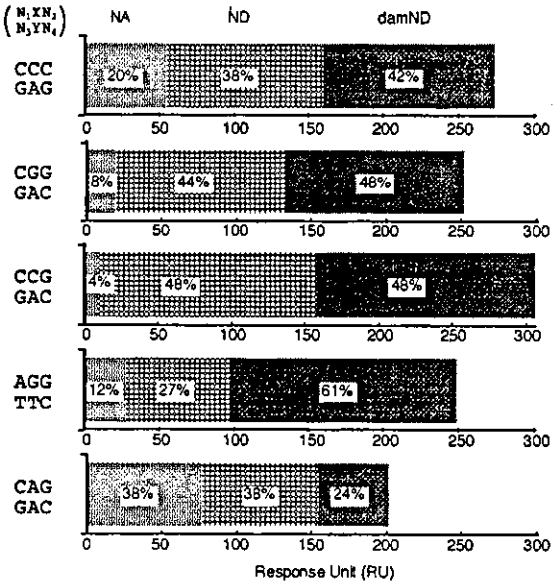

Figure 1. The sum of the responses obtained by damND, ND, and NA immobilized sensor surface at 180 sec after injection of 27mer 5'-d(GTT ACA GAA TCT N_1XN_2 AAG CCT AAT ACG)-3'/3'-d(CAA TGT CTT AGA N_3YN_4 TTC GGA TTA TGC)-5' (1 μM). Binding was measured in HBS-N (pH 7.4) containing 500 mM NaCl. Ratio of the response obtained by each sensor surfaces are shown in bar graph.

the component ratio of responses obtained by MLB immobilized surface, distinct differences were observed between individual mismatched base pairs, although the total response were almost the same for these mismatches. These results suggested that SPR fingerprinting obtained by MLB immobilized surface would be the effective way to differentiate the mismatched base pairs.

REFERENCES

1. Nakatani, K., Kobori, A., Kumasawa, H., Saito, I. (2004) *Bioorg. Med. Chem. Lett.*, **14**, 1105-1108.
2. Hagihara, S., Kumasawa, H., Hayashi, G., Kobori, A., Saito, I., Nakatani, K. (2004) *Nucleic Acids Res*, **32**, 273-286.
3. Kobori, A., Horie, S., Suda, H., Saito, I., Nakatani, K. (2004) *J. Am. Chem. Soc*, **126**, 557-562.

J|A|C|S
ARTICLES
Published on Web 01/03/2004

Nature of the Chemical Bond Formed with the Structural Metal Ion at the A9/G10.1 Motif Derived from Hammerhead Ribozymes

Yoshiyuki Tanaka,*,†,‡ Yasuhiro Kasai,† Shunsuke Mochizuki,§ Akihiro Wakisaka,§ Eugene H. Morita,∥,⊥ Chojiro Kojima,# Atsushi Toyozawa,‡ Yoshinori Kondo,‡ Masumi Taki,†,▽ Yasuomi Takagi,† Atsushi Inoue,▽ Kazuhiko Yamasaki,+ and Kazunari Taira*,†,▽

Contribution from the Gene Function Research Center, National Institute of Advanced Industrial Science and Technology (AIST), Central 4, 1-1-1 Higashi, Tsukuba Science City 305-8562, Japan, Graduate School of Pharmaceutical Sciences, Tohoku University, Aobayama, Sendai, Miyagi 980-8578, Japan, Environmental Molecular Science Group, AIST, Tsukuba, Ibaraki 305-8569, Japan, Integrated Center for Science, Ehime University, Matsuyama, Ehime 790-8566, Japan, Venture Business Laboratory, Ehime University, Matsuyama, Ehime 790-8577, Japan, Graduate School of Biological Science, Nara Institute of Science and Technology, Ikoma, Nara 630-0101, Japan, Department of Chemistry and Biotechnology, School of Engineering, The University of Tokyo, Hongo, Tokyo 113-8656, Japan, and Age Dimension Research Center, AIST, Tsukuba Science City 305-8566, Japan

Received June 22, 2003; E-mail: taira@chembio.t.u-tokyo.ac.jp; tanaka@mail.pharm.tohoku.ac.jp

Abstract: We have studied the interaction between metal ions and the metal ion-binding motif in hammerhead ribozymes, as well as the functions of the metal ion at the motif, with heteronuclear NMR spectroscopy. In this study, we employed model RNA systems which mimic the metal ion-binding motif and the altered motif. In $Co(NH_3)_6$(III) titrations, we observed large ^1H and ^{31}P chemical shift perturbations for the motif and found that outer-sphere complexation of $Co(NH_3)_6$(III) is possible for this motif. From the reinvestigation of our previous ^{15}N chemical shift data for Cd(II) binding, in comparison with those of organometallic compounds, we conclude that Cd(II) can form an inner-sphere complex with the nucleobase in the motif. Therefore, the A9/G10.1 site was found to accept both inner-sphere and outer-sphere complexations. The Mg(II) titration for a slightly different motif from the A9/G10.1 site (G10.1−C11.1 to A10.1−U11.1) revealed that its affinity to Mg(II) was drastically reduced, although the ribozyme with this altered motif is known to retain enzymatic activities. This observation suggests that the metal ion at these motifs is not a catalytic center of hammerhead ribozymes.

Introduction

Biologically active RNA molecules utilize metal ions to fold into specific conformation or to form a catalytic center. In the case of hammerhead ribozymes, there is a metal ion-binding motif (the A9/G10.1 site) in its conserved core region (Figure 1).[1−6] To understand the mechanism of hammerhead ribozymes, it is important to analyze the interaction between metal ions and the consensus sequences of hammerhead ribozymes.[7−16]

† Gene Function Research Center, AIST.
‡ Tohoku University.
§ Environmental Molecular Science Group, AIST.
∥ Integrated Center for Science, Ehime University.
⊥ Venture Business Laboratory, Ehime University.
Nara Institute of Science and Technology.
▽ The University of Tokyo.
+ Age Dimension Research Center, AIST.

(1) Pley, H. W.; Flaherty, K. M.; McKay, D. B. *Nature* **1994**, *372*, 68−74.
(2) Scott, W. G.; Murray, J. B.; Arnold, J. R.; Stoddard, B. L.; Klug, A. *Science* **1996**, *274*, 2065−2069.
(3) Murray, J. B.; Terwey, D. P.; Maloney, L.; Karpeisky, A.; Usman, N.; Beigelman, L.; Scott, W. G. *Cell* **1998**, *92*, 665−673.
(4) Tanaka, Y.; Morita, E. H.; Hayashi, H.; Kasai, Y.; Tanaka T.; Taira, K. *J. Am. Chem. Soc.* **2000**, *122*, 11303−11310.
(5) Tanaka, Y.; Kojima, C.; Morita, E. H.; Kasai, Y.; Yamasaki, K.; Ono, A.; Kainosho, M.; Taira, K. *J. Am. Chem. Soc.* **2002**, *124*, 4595−4601.
(6) Suzumura, K.; Yoshinari, K.; Tanaka, Y.; Takagi, Y.; Kasai, Y.; Warashina, M.; Kuwabara, T.; Orita, M.; Taira, K. *J. Am. Chem. Soc.* **2002**, *124*, 8230−8236.
(7) Ruffner, D. E.; Stormo, G. D.; Uhlenbeck, O. C. *Biochemistry* **1990**, *29*, 10695−10702.
(8) (a) Peracchi, A.; Beigelman, L.; Usman, N.; Herschlag, D. *Proc. Natl. Acad. Sci. U.S.A.* **1996**, *93*, 11522−11527. (b) Peracchi, A.; Beigelman, L.; Scott, E. C.; Uhlenbeck, O. C.; Herschlag, D. *J. Biol. Chem.* **1997**, *272*, 26822−26826. (c) Wang, S.; Karbstein, K.; Peracchi, A.; Beigelman, L.; Herschlag, D. *Biochemistry* **1999**, *38*, 14363−14378.
(9) (a) Tuschl, T.; Gohlke, C.; Jovin, T. M.; Westhof, E.; Eckstein, F. *Science*, **1994**, *266*, 785−789. (b) Bassi, G. S.; Mollegaard, N. E.; Murchie, A. I.; von Kitzing, E.; Lilley, D. M. J. *Nat. Struct. Biol.* **1995**, *2*, 45−55. (c) Sigurdsson, S. T.; Tuschl, T.; Eckstein, F. *RNA*, **1995**, *1*, 575−583. (d) Bassi, G. S.; Murchie, A. I.; Lilley, D. M. J. *RNA* **1996**, *2*, 756−768. (e) Bassi, G. S.; Murchie, A. I.; Walter, F.; Clegg, R. M.; Lilley, D. M. J. *EMBO J.* **1997**, *16*, 7481−7489.
(10) Hampel, K. J.; Burke, J. M. *Biochemistry* **2003**, *42*, 4421−4429.
(11) Scott, E. C.; Uhlenbeck, O. C. *Nucleic Acids Res.* **1999**, *27*, 479−484.
(12) Yoshinari, K.; Taira, K. *Nucleic Acids Res.* **2000**, *28*, 1730−1742.
(13) Nakamatsu, Y.; Warashina, M.; Kuwabara, T.; Tanaka, Y.; Yoshinari, K.; Taira, K. *Genes Cells* **2000**, *5*, 603−612.
(14) Murray, J. B.; Scott, W. G. *J. Mol. Biol.* **2000**, *296*, 33−41.
(15) Takagi, Y.; Warashina, M.; Stec, W. J.; Yoshinari, K.; Taira, K. *Nucleic Acids Res.* **2001**, *29*, 1815−1834.

10.1021/ja036826t CCC: $27.50

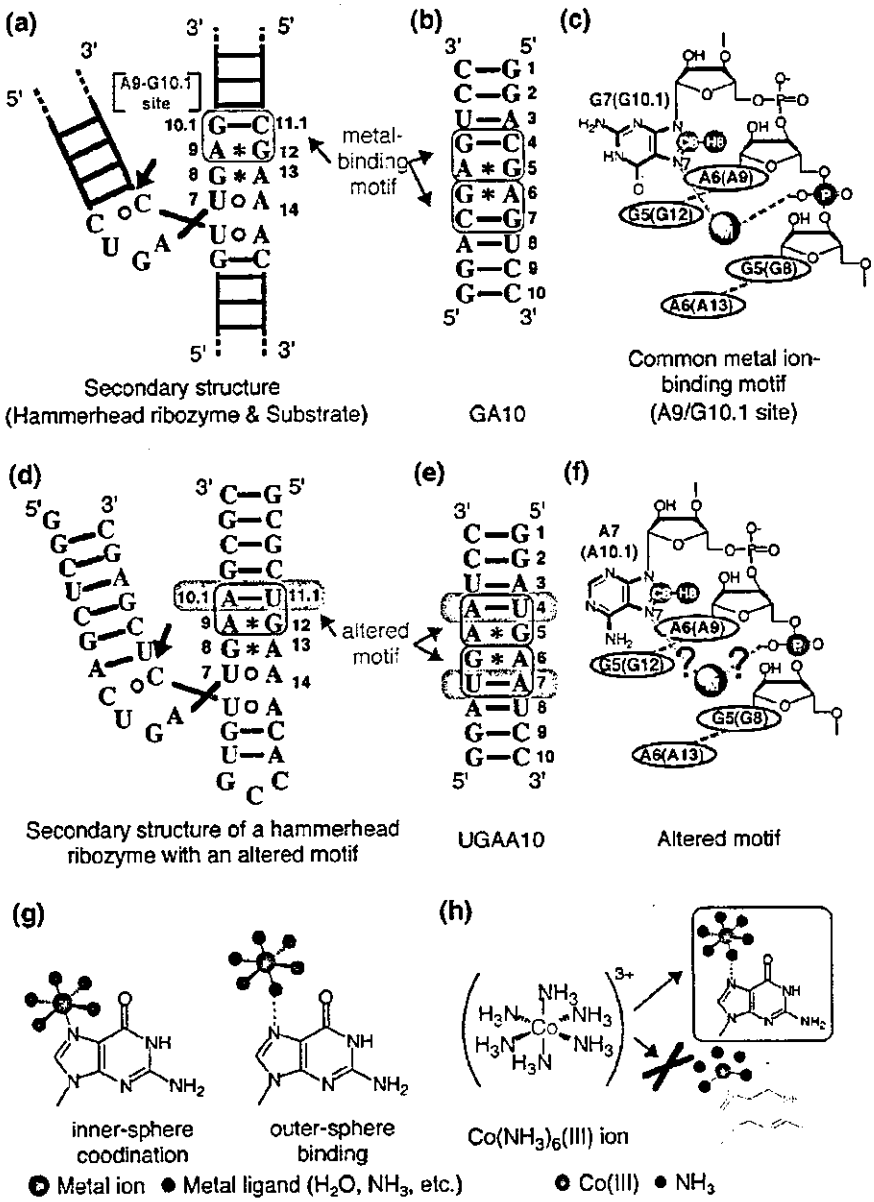

Figure 1. Sequences and metals. (a) Common sequences and a secondary structure of hammerhead ribozymes. (b) GA10 with numbering systems. (c) Schematic representation of the common metal ion-binding motif (the A9/G10.1 site) of hammerhead ribozymes. The residue numbers in GA10 are shown, and the residue numbers in hammerhead ribozymes are also shown in parentheses. (d) Sequences and the secondary structure of the hammerhead ribozyme with A10.1–U11.1, studied by Ruffner et al.[7] (e) UGAA10: A GA10 analogue with an altered motif. (f) Schematic representation of the altered motif. In (a), (b), (d), and (e), the common metal-binding motif (the A9/G10.1 site) and the altered motif are surrounded by magenta and blue lines, respectively. The substituted sequences are highlighted with magenta background. In (a) and (d), enzyme and substrate strands are shown in black and red, respectively, and the cleavage site is indicated by a black arrow. In (c) and (f), a metal ion is shown in a gray circle with a character "M" and is linked to binding sites via dashed lines. The tandem G–A pairs are indicated by black dashed lines with residue names. Watson–Crick base pairs, non-Watson–Crick base pairs, and sheared-type G–A pairs are indicated in bars, open circles, and asterisks. The nuclei monitored by 1D ^{31}P NMR spectra and 2D natural-abundance ^{1}H–^{13}C HSQC spectra are highlighted (P, red; C8, green; H8, red). In (g), metal ion recognition modes are illustrated (inner-sphere coordination and outer-sphere binding [hydrogen bonding through metal ligands]). In (h), $Co(NH_3)_6$(III) binding modes are illustrated. In the case of $Co(NH_3)_6$(III), an inner-sphere coordination of the Co(III) center to nucleobases is inhibited; however, outer-sphere binding is allowed because of exchange-inert metal ligands (NH_3).

Specifically, it is becoming important whether the metal ions at the A9/G10.1 site are catalytic metals (a catalytic center) or structural metals (structural constituents), since this metal ion is the most frequently observed metal ion throughout the crystal structures of hammerhead ribozymes.[1-6,8,11-16] It is also known that this metal ion-binding motif and very similar motifs appear in ribosomal RNAs.[17] Therefore, it is obviously important to study the interaction between metal ions and the metal ion-binding motif.

Recently, studies on the metal–biomacromolecule interaction became one of the topics in biology, and there have been several

(16) O'rear, J. L.; Wang, S.; Feig, A. L.; Beigelman, L.; Uhlenbeck, O. C.; Herschlag, D. *RNA* **2001**, *7*, 537–545.

(17) Gautheret, D.; Konings, D.; Gutell, R. R. *J. Mol. Biol.* **1994**, *242*, 1–8.

Table 1. Chemical Shift Perturbations upon Additions of Metal Ions[a]

sequences	metals	residue	C8/ppm	H8/ppm	ref.
r(GGACGAGUCC)$_2$ [GA10]	$MgCl_2$	G7	+0.5 (2.0 equiv)	+0.12 (9.0 equiv)	4
r(GGACGAGUCC)$_2$ [GA10]	$CdCl_2$	G7	+2.3 (5.0 equiv)	+0.38 (9.0 equiv)	5 and this work
r(GGACGAGUCC)$_2$ [GA10]	$Co(NH_3)_6Cl_3$	G7	+0.1 (2.0 equiv)	+0.25 (3.0 equiv)	this work
r(GGACGAGUCC)$_2$ [GA10]	$NaClO_4$	G7	+0.1 (230 mM)[b]	+0.12 (800 mM)[b]	this work
d(ATGGGTACCCAT)$_2$ [12mer]	$ZnCl_2$	G4	+2.5 (8.0 equiv)	+0.20 (8.0 equiv)	42
d(ATGGGTACCCAT)$_2$ [12mer]	$ZnCl_2$	G3	+1.5 (8.0 equiv)	+0.05 (8.0 equiv)	42
d(TGGT)	Pt(en)Cl_2[c]	G3	+1.1 (1.0 equiv)	+1.04 (1.0 equiv)	43
d(TGGT)	Pt(en)Cl_2[c]	G2	+0.2 (1.0 equiv)	+0.26 (1.0 equiv)	43

[a] Chemical shift perturbations were listed in ppm with molar equivalencies to duplexes (GA10 and 12mer) or a single strand of d(TGGT). Plus values indicate lower field shift. [b] Chemical shift perturbations from the basal solutions are listed. [c] Pt(en)Cl_2 (en = ethylenediamine) forms covalent complex d(TGGT)·Pt(en) with the two successive guanosines of d(TGGT).[43,44]

studies on this topic using solution NMR techniques. In the case of nucleic acids, there have been studies on the interaction between metal ions and nucleic acids.[4−6,18−23] DeRose and coworkers demonstrated that in hammerhead ribozymes there is at least one nitrogen atom which is coordinated to Mn(II), with the EPR spectrum measurements of Mn(II), and they suggested the Mn(II) coordination site on the ribozyme.[24−26] The solution NMR technique provides us with a more rigid answer for a metal ion-binding site in the RNA molecule.[4−6,18−23] Despite those extensive works, there is no direct evidence for what kind of chemical bonds were formed between metal ions and nucleobases in ribozymes. In the case of organometallic complexes for organic synthesis, it has been demonstrated that metal ligands dramatically influence reactivities, catalytic activities, and regio- and stereoselectivities of chemical reactions.[27] Thus, for understanding the mechanism of the action of hammerhead ribozymes, it is important to know not only what ligands are on the metal center, but also what kinds of chemical bonds are formed between the metal center and ligands. In our previous studies using heteronuclear multidimensional NMR spectroscopy, we used GA10 as a model RNA oligomer mimicking the metal ion-binding motif of hammerhead ribozymes (Figure 1) and found that Cd(II) specifically bound to the N7 nuclei of the G7 residue [N7(G7)].[4,5] However, we could not definitely conclude whether the binding of Cd(II) to N7(G7) was direct coordination or not.[4,5] This is because we could not detect the scalar coupling between ^{113}Cd(II) and ^{15}N7(G7),[5] as were the cases for other nucleoside−metal ion systems.[28,29] For further information, it is interesting to introduce several kinds of metal ion sources with different characters, such as $Co(NH_3)_6Cl_3$, $NaClO_4$, $MnCl_2$, $EuCl_3$, and $TbCl_3$.

The $Co(NH_3)_6$(III) ion is known as a model for a hexahydrated Mg(II) ion, since the ionic radius of $Co(NH_3)_6$(III), including NH_3 ligands, is very close to that of hexahydrated magnesium ions $[Mg(H_2O)_6]$.[30] In addition, $Co(NH_3)_6$(III) ions are ligated with exchange-inert NH_3 ligands, and then nucleobases cannot be directly coordinated to the Co(III) center of this complex (Figure 1g,h).[30] Therefore, it can be used for a control metal ion that cannot form an inner-sphere coordination.[30] Sodium ion is used to monitor the degree of ionic strength-dependent chemical shift changes. The Mn(II) ion is used to demonstrate whether metal ions are surely located near the nucleobase, since its paramagnetic property causes signal broadening around the binding site in a distance-dependent manner.[18−20] The Eu(III) and Tb(III) ions were also used as a fluorescent probe. Using these data as well as those of Cd(II) and Mg(II), we tried to reveal what kinds of chemical bonds are formed between a metal ion and the metal ion-binding motif in hammerhead ribozymes. The role of the metal ion at this motif was also investigated using a nucleotide-substituted RNA. Ruffner et al. indicated that the hammerhead ribozyme with the A10.1−U11.1 pair retained 30% cleavage activity relative to that with a common G10.1−C11.1 pair.[7] If the metal ion at the A9/G10.1 site is a catalytic metal of hammerhead ribozymes, the altered motif with A−U pair at the 10.1 and 11.1 positions should capture a metal ion. To clarify this point as well as the sequence requirements for the metal ion recognition, we performed titration experiments of the altered motif with Mg(II), the most probable cofactor in physiological conditions.[31]

Results

Titration Experiments with ^{1}H and ^{31}P NMR Spectra. In previous studies, we have demonstrated that divalent cations, such as Mg(II) and Cd(II), were able to bind to the metal ion-binding motif through the N7 nucleus of G7 in GA10 using ^{1}H, ^{13}C, and ^{15}N chemical shift perturbation (Tables 1 and 2).[4,5] In those studies, large chemical shift perturbations were observed for N7, C8, and H8 resonances of the G7 residues (−19.6, 2.3, and 0.38 ppm, respectively) upon the addition of Cd(II) ions (Tables 1 and 2).[4,5] Therefore, it was suggested that Cd(II) and Mg(II) ions directly coordinated to N7(G7). To clarify this situation in detail, we employed $Co(NH_3)_6$(III) ions, since exchange-inert NH_3 ligands prevent an inner-sphere coordination of the Co(III) center to nucleobases. If the direct coordination of a metal center is a prerequisite for the metal ion binding to the motif, $Co(NH_3)_6$(III) ions cannot bind to the motif. Contrary

(18) Allain, F. H.-T.; Varani, G. *Nucleic Acids Res.* **1995**, *23*, 341−350.
(19) Hansen, M. R.; Simorre, J. P.; Hanson, P.; Mokler, V.; Bellon, L.; Beigelman, L.; Pardi, A. *RNA* **1999**, *5*, 1099−1104.
(20) Rüdisser, S.; Tinoco, I., Jr. *J. Mol. Biol.* **2000**, *295*, 1211−1223.
(21) Butcher, S. E.; Allain, F. H.-T.; Feigon, J. *Biochemistry* **2000**, *39*, 2174−2182.
(22) Schmitz, M.; Tinoco, I., Jr. *RNA* **2000**, *6*, 1212−1225.
(23) Maderia, M.; Hunsicker, L. M.; DeRose, V. J. *Biochemistry* **2000**, *39*, 12113−12120.
(24) (a) Morrissey, S. R.; Horton, T. E.; Grant, C. V.; Hoogstraten, C. G.; Britt, R. D.; DeRose, V. J. *J. Am. Chem. Soc.* **1999**, *121*, 9215−9218. (b) Morrissey, S. R.; Horton, T. E.; DeRose, V. J. *J. Am. Chem. Soc.* **2000**, *122*, 3473−3481.
(25) Hoogstraten, C. G.; Grant, C. V.; Horton, T. E.; DeRose, V. J.; Britt, R. D. *J. Am. Chem. Soc.* **2002**, *124*, 834−842.
(26) Hunsicker, L. M.; DeRose, V. J. *J. Inorg. Biochem.* **2000**, *80*, 271−281.
(27) (a) Hegedus L. S. *Transition Metals in the Synthesis of Complex Organic Molecules*, 2nd ed.; University Science Books: Sausalito, CA, 1999. (b) Imahori, T.; Uchiyama, M.; Sakamoto, T.; Kondo, Y. *Chem. Commun.* **2001**, *23*, 2450−2451. (c) Uchiyama, M.; Miyoshi, T.; Kajihara, Y.; Sakamoto, T.; Otani, Y.; Ohwada, T.; Kondo, Y. *J. Am. Chem. Soc.* **2002**, *124*, 8514−8515.
(28) Buchanan, G. W.; Stothers, J. B. *Can. J. Chem.* **1982**, *60*, 787−791.
(29) Buchanan, G. W.; Bell, M. J. *Can. J. Chem.* **1983**, *61*, 2445−2448.
(30) Cowan, J. A. *J. Inorg. Biochem.* **1993**, *49*, 171−175.
(31) Zhou, J.-M.; Zhou, D.-M.; Takagi, Y.; Kasai, Y.; Inoue, A.; Baba, T.; Taira, K. *Nucleic Acids Res.* **2002**, *30*, 2374−2382.

Table 2. Summary of ^{15}N NMR Data

metal ligands (ref.)	[ligand]/mM	metals	residue	$\Delta^{15}N^a$/ppm	$^1J_{N-M(II)}{}^b$/Hz
r(GGACGAGUCC)$_2$ [GA10] (5)	0.45	$CdCl_2$	G7	−19.6 (6.0 equiv)	not detected
guanosine monomer (28)	500	$Zn(NO_3)_2$	n.a.[c]	−20.1 (1.0 equiv)	n.a.
guanosine monomer (28)	500	$Hg(NO_3)_2$	n.a.	−20.5 (1.0 equiv)	not reported
inosine monomer (29)	1000	$Zn(NO_3)_2$	n.a.	−15.2 (0.7 equiv)	n.a.
inosine monomer (29)	1000	$Hg(NO_3)_2$	n.a.	−4.8 (0.75 equiv)	not detected
1-methylimidazole[d] [MI] (33)	240	$Cd(NO_3)_2$	n.a.	−28.7[d] (0.2 equiv)	not reported
1-methylimidazole[d] [MI] (33)	350	$Zn(NO_3)_2$	n.a.	−46.0[d] (0.22 equiv)	n.a.
β-lactamase (35)	0.8	$CdCl_2$	His[e]	n.r.[f]	~78−216
EDTA (36)	400	$CdCl_2$	n.a.	+3.3 (1.9 equiv)	81

[a] Chemical shift perturbations of N7(guanosine), N3(1-methylimidazole), and tertiary amine nitrogens (EDTA) from the unmetalated state. Minus and plus values indicate higher and lower field shifts, respectively. [b] *J*-coupling between metalated nitrogens (^{15}N) and metal ions ($I = 1/2$), such as ^{113}Cd and ^{199}Hg. Only absolute values are indicated. [c] Not applicable. [d] In the equilibrium system of 1-methylimidazole [MI] and metal ions [M(II)], the ^{15}N chemical shift of N3 reflects an average value of those from free, protonated, and metal complexes (M(II)-MI, M(II)-2·MI, M(II)-3·MI, M(II)-4·MI, and so on). Therefore, chemical shift values of 1-methylimidazole are average values of these species. [e] Four of seven histidines were metalated, but residue numbers in the amino acid sequence were not reported. [f] Not reported. However, in β-lactamase-Cd(II) system, ranges of ^{15}N chemical shifts of metalated and unmetalated residues were overlapped, and ^{15}N chemical shift perturbations due to a metalation were estimated to be small. For the interpretations of the ^{15}N NMR chemical shift, Alei and co-workers presented interesting data on the ^{15}N chemical shift of 1-methylimidazole.[33] Chemical structure of the five-membered ring of the guanosine base is the same as 1-methylimidazole, and N7 of guanosine corresponds to N3 of 1-methylimidazole (Figure 7). They indicated that the ^{15}N chemical shift of N3, a metal ion-coordination site of 1-methylimidazole, was perturbed toward high field (~15−30 ppm) upon the complexation with Cd(II) in H_2O.[33] In this system, it seems difficult for an imidazole ring to form stable outer-sphere complexes with Cd(II) (the outer-sphere binding via water molecules of Cd(II) ligands). since 1-methylimidazole is a monodentate ligand. In other words, the observed complex is thought to be a coordination compound, and the higher field shift of the N3 resonance of 1-methylimidazole is due to an inner-sphere coordination of the N3 atom to Cd(II). Therefore, when the imidazole ring nitrogen coordinates to transition metal ions, such as Cd(II) and Zn(II), the ^{15}N chemical shift can be perturbed toward high field.

to this, if $Co(NH_3)_6$(III) ions can bind to the motif, it is deduced that this metal ion-binding motif allows the metal ion binding through the metal ligands, including water molecules. To estimate ionic strength-dependent chemical shift changes, titration experiments with $NaClO_4$ were also performed. On the basis of the above concepts, we performed titration experiments with $Co(NH_3)_6Cl_3$ and $NaClO_4$, using one-dimensional (1D) ^1H and ^{31}P NMR spectra (Figure 2), as well as those of $CdCl_2$ (an example for tight binding).

Contrary to our early prediction, titration data with 1D ^1H and ^{31}P NMR spectra indicated $Co(NH_3)_6$(III) ion binding to GA10, since large chemical shift perturbations were observed for the resonances in the motif (the H8 resonance of the G7 residue [H8(G7)], phosphorus of the A6 residue [P(A6)], and the neighboring residues in GA10) (Figure 2). In contrast to the titrations for $Co(NH_3)_6$(III) and Cd(II), sodium ion titration curves of ^1H and ^{31}P resonances were almost linearly increased against the concentration of $NaClO_4$, except for those at the 5′ end (Figure 2). It was also found that ionic strength-dependent chemical shift perturbations for proton resonances were small (the maximum perturbation: 0.0002 ppm per 1 molar equivalent $NaClO_4$ for the H6 proton of the C4 residue) and negligible for the titration data of Cd(II) and $Co(NH_3)_6$(III). It was found that metal ion binding to the motif was not a simple electrostatic interaction, and sodium ions do not bind to the motif in a site-specific manner. This is consistent with the result by Herschlag's group that monovalent lithium ions did not bind to the motif during the catalytic reaction of hammerhead ribozymes.[16] Therefore, the chemical shift perturbations by Cd(II) and $Co(NH_3)_6$(III) titrations were due to their site-specific binding to GA10.

Intermolecular NOEs between GA10 and $Co(NH_3)_6$(III). We tried to exclude the possibility that the chemical shift perturbations for $Co(NH_3)_6$(III) titrations were due to the secondary effect from $Co(NH_3)_6$(III) binding to somewhere outside the motif. For this purpose, we measured two-dimensional (2D) $^1H-^1H$ NOESY spectra (90% H_2O, 10% D_2O). In the spectrum, several intermolecular NOEs were observed between protons of $Co(NH_3)_6$(III) ions and base protons of GA10 (Figure 3). Especially between the $Co(NH_3)_6$(III) ions and H8(G7) was one of the strongest intermolecular NOEs, and other NOEs were observed for the base protons and amino protons around the A9/G10.1 site (Figure 3a). In the upper panel of Figure 3a, possible NOE counterparts for $Co(NH_3)_6$(III) are indicated. A strong intermolecular NOE was also observed between the imino proton of the G7 residue and the NH_3 ligands (Figure 3b). It was surely demonstrated that the $Co(NH_3)_6$(III) ion bound to the A9/G10.1 site selectively.

$^1H-^{13}C$ HSQC Spectra of GA10. We recorded 2D $^1H-^{13}C$ HSQC spectra with or without metal salts such as $Co(NH_3)_6Cl_3$, $CdCl_2$, and $NaClO_4$ (Figure 4). As previously shown,[4,5] Cd(II) ions significantly perturbed the C8(G7) resonance toward low field (Figure 4a,b). In contrast, $Co(NH_3)_6Cl_3$ and $NaClO_4$ only perturbed the C8(G7) resonance within an error range of absolute chemical shift values (Figure 4c−f). From the titration and NOE data for the GA10−$Co(NH_3)_6$(III) system, $Co(NH_3)_6$(III) is thought to bind to N7(G7) via NH_3 ligand-mediated hydrogen bonding (outer-sphere binding); however, this outer-sphere binding did not affect the chemical shift of C8(G7). In other words, the lower field shift of C8(G7) upon the addition of Cd(II) is not explainable without an inner-sphere coordination of a metal ion to N7(G7). It was also found that sodium ions did not affect the chemical shifts of C8 atoms of all residues significantly.

Effects of a Paramagnetic Metal Ion. To exclude the possibility that the chemical shift perturbations for C8(G7) upon addition of Cd(II) and Mg(II) merely reflect the conformational changes due to their binding to allosteric sites, we have monitored signal broadening due to paramagnetic Mn(II) ion binding. This technique indicates that Mn(II) ions surely locate near the site where the resonances were broadened since the signal broadening occurs in a distance-dependent manner.[18−20] It is also known that Mn(II) and Cd(II) ions belong to relatively soft acids, according to the hard and soft acids and bases (HSAB) rule, and kinetic and thermodynamic behavior of Mn(II) is similar to that of Cd(II) in the catalytic reaction of ham-

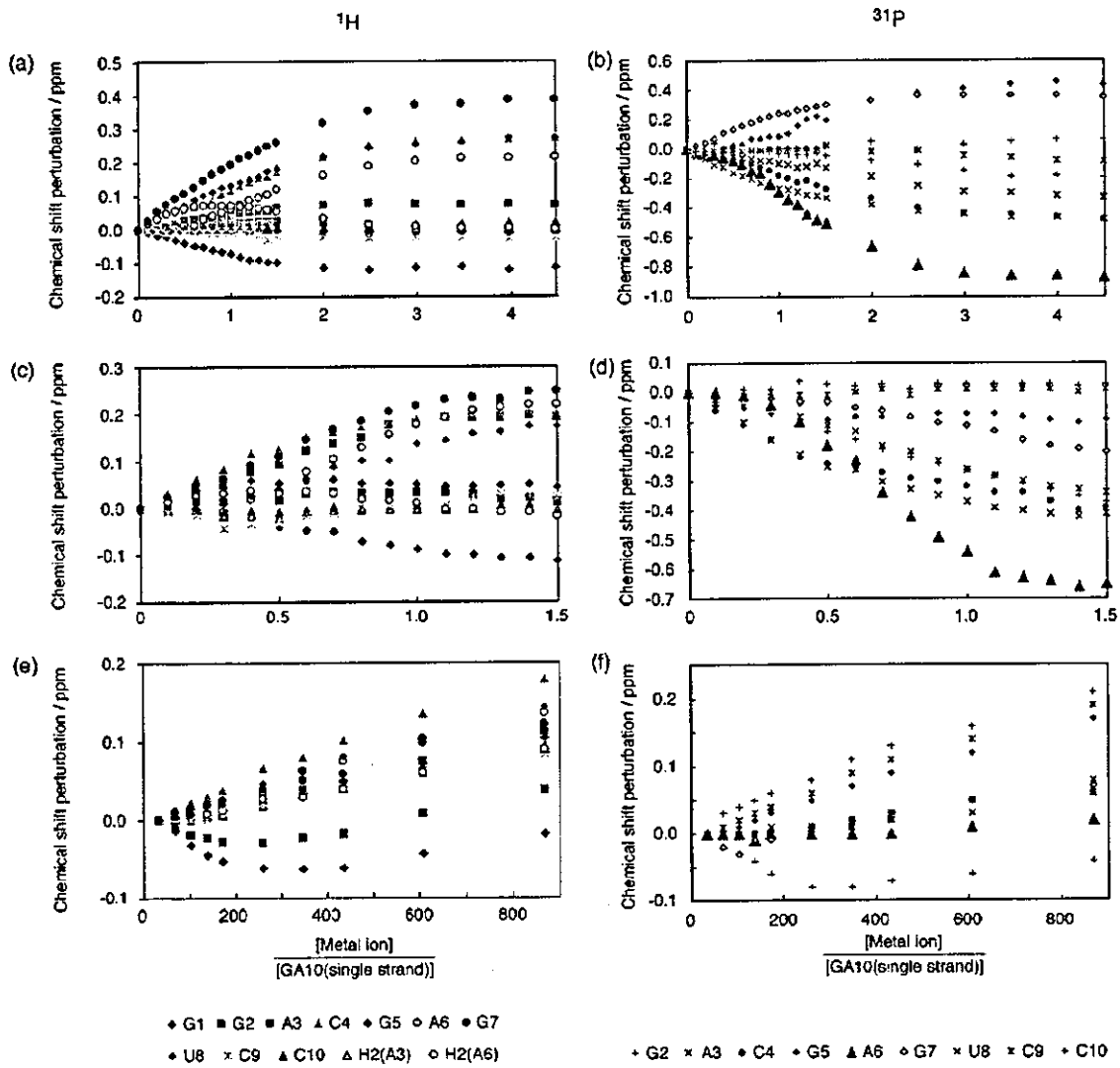

Figure 2. Chemical shift perturbations for base protons [H8(purine), H6(pyrimidine), and H2(adenosine)] against a molar ratio ([metal ion]/[GA10(single strand)]). In (a), (c), and (e), those of ^{1}H resonances were plotted for Cd(II), $Co(NH_3)_6$(III), and sodium ions, respectively. In (b), (d), and (f), those of ^{31}P resonances were plotted for Cd(II), $Co(NH_3)_6$(III), and sodium ions, respectively. For Cd(II) titrations, various concentrations of $CdCl_2$ were added to the solution containing 1.5 mM GA10(single strand) and 40 mM $NaClO_4$. For $Co(NH_3)_6$(III) titrations, various concentrations of $Co(NH_3)_6Cl_3$ were added to the solution containing 2.0 mM GA10(single strand) and 40 mM $NaClO_4$. For sodium titrations, various concentrations of additional $NaClO_4$ were added to the solution containing 1.1 mM GA10(single strand) and 40 mM $NaClO_4$. Typical 1D ^{1}H, ^{31}P NMR spectra were recorded on Bruker DMX 750 spectrometer at 313 K. For ^{1}H NMR spectra, spectral width was 10 000 Hz digitized into 16 384 complex points; 128 scans were averaged. For ^{31}P NMR spectra, spectral width was 10 000 Hz digitized into 16384 complex points; 1024 scans were averaged. We confirmed that resonance assignments were consistent with other spectra, such as 2D ^{1}H−^{1}H NOESY, ^{1}H−^{13}C HSQC, and ^{1}H−^{31}P HMQC NOESY spectra.

merhead ribozymes.[8-12,15,16] Accordingly, Mn(II) is regarded as a model of Cd(II). From this experiment, broadening of H8-(G7) was evident (Figure 5). It was demonstrated that Mn(II) was surely located near H8(G7). Therefore, Cd(II) is also thought to be located near N7(G7), and the chemical shift perturbation of H8, C8, and N7 of G7 should be due to the metal ion binding to N7(G7).

Sequence Requirements for the Metal Ion Binding. We have also tested whether the G7 residue (G10.1 in hammerhead ribozymes) can be replaced by adenosine without a loss of the affinities for divalent cations. In the metal ion-binding motif of GA10, N7(G7) was shown to be a Cd(II)-binding site, whereas O6(G7) was not.[5] Although there is one example where O6-(G10.1) is utilized as a metal ligand in the crystal structure of the hammerhead ribozyme−Co(II) complex,[3] it is not a definitive requirement for other systems.[1,2] Therefore, we thought that the guanosine residue at the G10.1 position is able to be substituted by an adenosine residue. Then, we synthesized the RNA oligomer, UGAA10:rGGAUGAAUCC, and measured the NMR spectra. It had been demonstrated that UGAA10 forms a duplex with sheared type G−A pairs in tandem at the middle of the duplex, and the UGAA sequence took a similar structure to that of r(GGGCUGAAGCCU)$_2$ by Heus et al.[32] It is also known that the hammerhead ribozyme with A10.1−U11.1

(32) (a) Tanaka, Y.; Kasai, Y.; Morita, E. H.; Kojima, C.; Toyozawa, A.; Yamasaki, K.; Taira, K.; Kondo Y. *Nucleic Acids Res.* **2003**, (Suppl. 3), 45−46. (b) Heus, H. A.; Wijmenga, S. S.; Hoppe, H.; Hilbers, C. W. *J. Mol. Biol.* **1997**, *271*, 147−158.

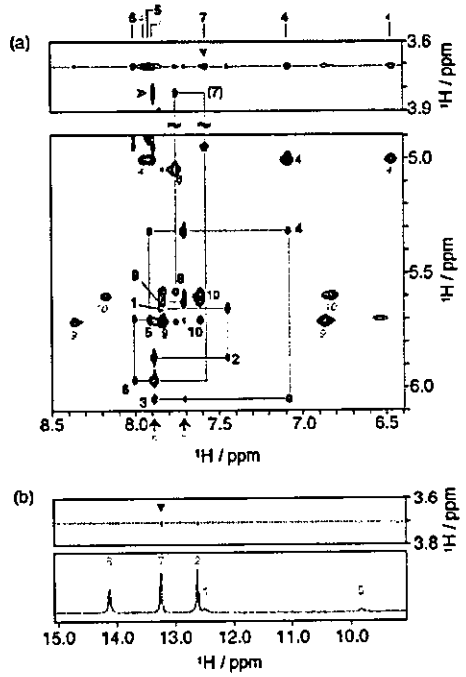

Figure 3. 2D ^{1}H–^{1}H NOESY spectrum in the presence of 1 molar equivalent of $Co(NH_3)_6Cl_3$ to the motif. The solution contained 3.4 mM GA10, 40 mM $NaClO_4$, and 3.4 mM $Co(NH_3)_6Cl_3$. The chemical shift of NH_3 ligands of $Co(NH_3)_6$(III) are indicated by red dashed lines. (a) NOE cross-peaks from $Co(NH_3)_6$(III) to GA10 (upper panel) and sequential NOE between base protons and anomeric protons (upper and lower panels) are presented. These intraresidue NOE cross-peaks were labeled with their residue number. The underlined numbers and green italic numbers are intraresidue H5–H6 cross-peaks and H5 amino protons cross-peaks for the corresponding residue number, respectively. Below the lower panel of (a), black arrows indicate the presence of H2 resonances on the corresponding chemical shift, with the residue numbers (orange numbers). NOE counterparts for $Co(NH_3)_6$(III) are also indicated above the upper panel of (a), and that of H8(G7) is indicated with a red arrowhead. We assigned the resonance at 3.81 ppm as H1′ of G7, since it is well-known that the H1′ resonances of the guanosine in the C–G pair, which is adjacent to a sheared type G–A pair in the same arrangement as the A9/G10.1 site, always resonated at an extraordinarily high field.[41] Katahira et al. assigned ^{1}H resonances of the same sequence as GA10 in the absence of $Co(NH_3)_6$(III) (H1′(G7) at 4.14 ppm for a solution containing 1.8 mM GA10, 20 mM sodium-phosphate buffer pH 7.0, and 150 mM NaCl, at 306 K).[41b] Heus and Pardi assigned ^{1}H resonances of the RNA oligomer r(GGG*CGCAA*GCCUUAU), including *GCAA* loop with a *C–G* closing base pair, adjacent to a sheared type G–A pair in the loop (H1′(G9) at approximately 3.7 ppm for a solution containing 1.9 mM RNA, 10 mM sodium phosphate buffer pH 6.8, and 100 mM NaCl at 298 K).[41a] It should be noted that in the absence of $Co(NH_3)_6$(III), H1′-(G7) of GA10 resonated at 3.99 ppm (1.2 mM GA10, 40 mM NaCl, pH 6 at 313 K).[39] Therefore, the chemical shift of H1′(G7) is significantly dependent on the measurement conditions, and slightly different chemical shifts for Katahira's conditions and ours are probably attributed to the differences in conditions. We have also confirmed this assignment by monitoring the NOE cross-peak (an open arrowhead) with H2(A6) (7.89 ppm), as Katahira et al. showed.[41b] This NOE cross-peak was observed in all 2D ^{1}H–^{1}H NOESY spectra in D_2O in the presence and absence of $CdCl_2$ and $Co(NH_3)_6Cl_3$.[39] In (b), 1D ^{1}H NMR spectrum of an imino proton region (lower panel) and NOE cross-peaks between $Co(NH_3)_6$(III) and imino protons are presented. In the lower panel of (b), residue numbers of imino protons are indicated. In the upper panel of (b), the cross-peak between imino proton of G7 and $Co(NH_3)_6$(III) is pointed to with a red arrowhead. In the NOESY spectrum, weak NOE cross-peaks from $Co(NH_3)_6$(III) were observed for nonspecific sites at this threshold. However, this phenomena might be a general feature of this experiment, since nonspecific NOEs from $Co(NH_3)_6$(III) were observed in other studies as well.[21,22] A 2D ^{1}H–^{1}H NOESY spectrum was recorded on Bruker DMX750 at 293 K; 4096*2048 complex points for a spectral width of 15 700*15 000 Hz.

instead of G10.1–C11.1 retains 30% cleavage activity, relative to the hammerhead ribozyme with the common G10.1–C11.1 pair.[7] This altered sequence motif is the same as that in UGAA10. Therefore, if the metal ion at A9/G10.1 and the corresponding site is a catalytic metal, this altered motif in UGAA10 should also capture divalent cations. However, chemical shift perturbations for UGAA10 were much less than those observed for GA10 upon the addition of 1 molar equivalent of $MgCl_2$ to the metal ion-binding motif (Figure 6). The maximum chemical shift perturbation of base protons in UGAA10 was observed for H8(G2) (0.03 ppm), the distal site from the putative metal ion-binding site (A7) (Figure 6). In addition, this perturbation is much smaller than those due to the specific binding of metal ions to GA10 (0.38 ppm for H8(G7) in Cd(II) titrations). Therefore, it is plausible that the chemical shift perturbations of the proton resonances in UGAA10 merely reflect changes in surrounding environments and cannot be attributed to specific binding of Mg(II). It is also known that nonspecific binding of divalent cations to backbone phosphates as counterions can occur at this concentration.[5] Therefore, the affinity between the motif in UGAA10 and Mg(II) is comparable to or lower than that between backbone phosphates and counterions of divalent cations. Accordingly, we can conclude that this altered motif with an adenosine residue at 10.1 position was not sufficient to capture divalent cations. From this result, in conjunction with sequence requirements for the cleavage reaction of hammerhead ribozymes,[7] it was suggested that the role of the metal ion at the A9/G10.1 site is not a catalytic metal, but a structural metal for the folding of hammerhead ribozymes.

Discussion

Investigations for $Co(NH_3)_6$(III) Binding. Intermolecular NOEs between $Co(NH_3)_6$(III) ions and the motif surely indicated that the $Co(NH_3)_6$(III) ion binds to the metal ion-binding motif (the A9/G10.1 site) (Figure 3). In addition, the binding isotherms of ^{1}H resonances for $Co(NH_3)_6$(III) titrations indicated biphasic (two-step) transitions, which means that two $Co(NH_3)_6$(III) ions were captured by GA10 at the metal ion-binding motif (Figure 2). This phenomenon is the same as in the GA10–Cd(II) system in which the binding isotherms are biphasic, and two Cd(II) ions bind to a GA10 duplex.[5] It should be noted that $Co(NH_3)_6$(III) titration curves for H8(A6) and H2(A6) significantly deviated from a monophasic transition curve and cannot be explained without biphasic transitions, as was the case for GA10–Cd(II) system.[5] It was also found that the overall binding isotherms of ^{1}H- and ^{31}P resonances for Cd(II) and $Co(NH_3)_6$(III) titrations were similar to each other. The resonances for the specific sites (H8(G7) and P(A6)) were especially similar to each other, although degrees of perturbations for the above resonances and titration curves for some resonances were different to some extent (Figure 2).

These data indicate that the binding sites of both $Co(NH_3)_6$-(III) and Cd(II) ions are similar or the same. Unfortunately, we could not completely exclude the possibility that $Co(NH_3)_6$(III) bound to O6(G7) or neighboring sites except for N7(G7). However, it is plausible that one of the binding sites for $Co(NH_3)_6$(III) ions is N7(G7) because of many similarities of the binding isotherms for both $Co(NH_3)_6$(III) and Cd(II) ions at this moment. Therefore, $Co(NH_3)_6$(III) is thought to be able to bind to the motif through the ligand-mediated hydrogen

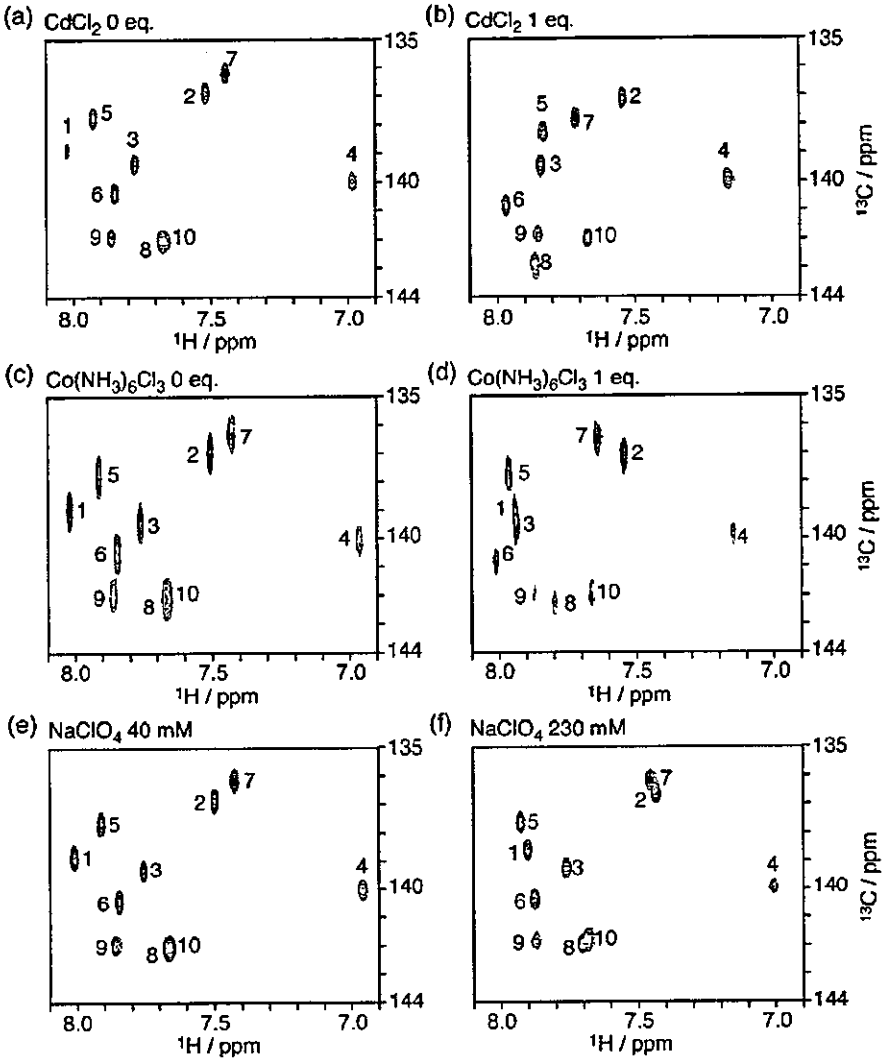

Figure 4. 2D $^1H-^{13}C$ HSQC spectra with or without metal ions. Panels (a) and (b) indicate spectra of basal solution (2.4 mM GA10(single strand), 40 mM $NaClO_4$) and that in the presence of $CdCl_2$ (2.4 mM GA10(single strand), 40 mM $NaClO_4$, and 2.4 mM $CdCl_2$). Panels (c) and (d) indicate spectra of basal solution (2.0 mM GA10(single strand), 40 mM $NaClO_4$) and that in the presence of $Co(NH_3)_6Cl_3$ (2.0 mM GA10(single strand), 40 mM $NaClO_4$, and 2.0 mM $Co(NH_3)_6Cl_3$). Panels (e) and (f) indicate spectra of basal solution (3.5 mM GA10(single strand), 40 mM $NaClO_4$) and that in the presence of excess $NaClO_4$ (3.5 mM GA10(single strand) and 230 mM $NaClO_4$). Intraresidue cross-peaks between H8 and C8 nuclei are labeled with their residue numbers, and that between H8(G7) and C8(G7) are indicated by red circles. In (a), (b), (e), and (f), spectra were recorded on Bruker DMX750 at 313 K; 1024*128 real points for a spectral width of 7003*5659 Hz. In (c) and (d), the point resolution was reduced to 1024*64 real points for the same spectral width since spectra were broadened upon the addition of 1 molar equivalent of $Co(NH_3)_6Cl_3$.

bonding (outer-sphere binding) (Figures 2–4). On the other hand, crystal structures indicate that several metal ions, such as Mn(II) and Co(II), can bind to the motif via an inner-sphere coordination to N7(G10.1) of hammerhead ribozymes.[1,3] Accordingly, the A9/G10.1 site is a motif which allows two kinds of binding modes, i.e., an inner-sphere coordination[1,3] and outer-sphere binding via metal ligands.

More importantly, the chemical shift of C8(G7) was not affected by the $Co(NH_3)_6$(III) ion binding (Figure 4c,d and Table 1), which means that hydrogen bonding between NH_3 ligands and the N7(G7) did not perturb the resonance of C8(G7) or other carbon resonances. In contrast, chemical shift values of both C8(G7) and H8(G7) were selectively perturbed upon the addition of Cd(II) and Mg(II) (Figure 4a,b and Table 1),[4] which can potentially coordinate to N7(G7). Together with the above data, simultaneous large lower field shift of C8 and H8 resonances of G7 cannot be explained without an inner-sphere coordination of a metal ion to N7(G7), although the resonance of C8(G7) for $Co(NH_3)_6$(III) titrations might be unchanged due to some cancellation by chance.

Reinvestigations of ^{15}N NMR Data. In our previous publication, we observed a higher field shift by 19.6 ppm for the ^{15}N resonance of N7(G7) without a detectable *J*-coupling between ^{15}N and ^{113}Cd(II) (Table 2).[5] The same phenomena were observed for the cases of guanosine–^{199}Hg(II) complex in dimethyl sulfoxide (DMSO) solution (Table 2).[28] In those studies, it was thought that guanosine and inosine were the ligands for the metal ions, and these nucleosides directly coordinated to the metal ions.[28,29] However, there has been no direct evidence that indicates the formation of the coordination

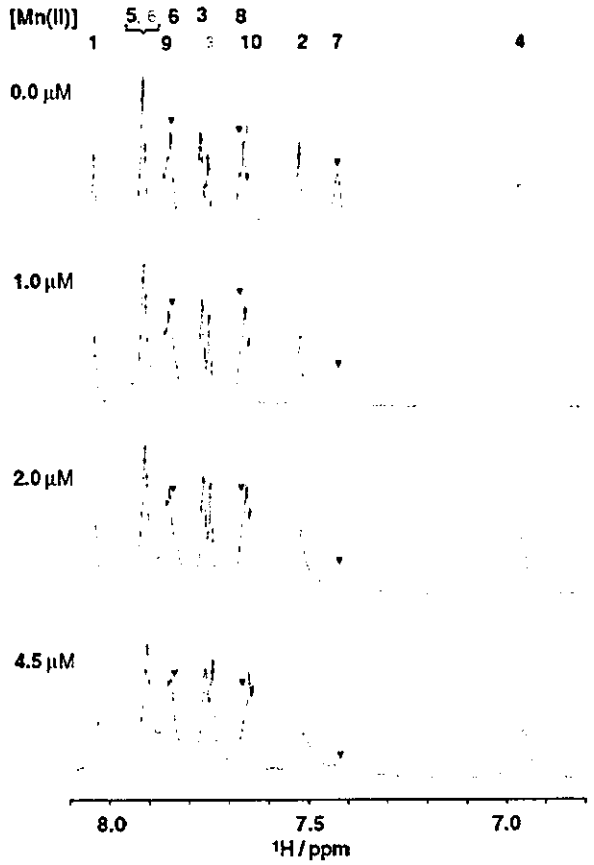

Figure 5. 1D ^{1}H NMR spectra with increasing $MnCl_2$ concentration. Concentration of $MnCl_2$ for each spectrum is indicated on the left of each spectrum. Signal broadening was observed for H8(G7) (red arrowhead). Signal intensities of H8(A6) and H6(U8) (black arrowheads) seemed to be decreased as well. Assignments of base protons are indicated with their residue numbers, and small orange characters indicate H2 resonances of the corresponding residue.

compound for the above systems. We then tried to detect what kind of complex is formed between Cd(II) and a guanosine monomer in DMSO by means of a specially designed mass spectrometer using an electrospray interface.[34] In this mass spectrometry, we can detect charged clusters that are present beforehand in solution.[34b] For example, even solvated ions such as lithium ion–methanol and cesium ion–methanol clusters were detected with this system.[34b]

In the DMSO solution of Cd(II) and guanosine (the Cd(II)–guanosine–DMSO system), we detected several complexes of three components (Cd(II), guanosine, and DMSO). The major complexes of Cd(II)–guanosine–DMSO were 1:1:3 (*M*/Z: 315.4), 1:1:4 (*M*/Z: 354.4), and 1:1:5 (*M*/Z: 393.4) complexes, which may possibly indicate Cd(II) complexes with the ligands in tetrahedral, square pyramidal, and octahedral geometries, respectively (unpublished data). Although other ternary complexes with different molar ratios were detected, their populations were much less than the 1:1:3, 1:1:4, and 1:1:5 complexes. It was indicated that guanosine directly coordinates to a soft

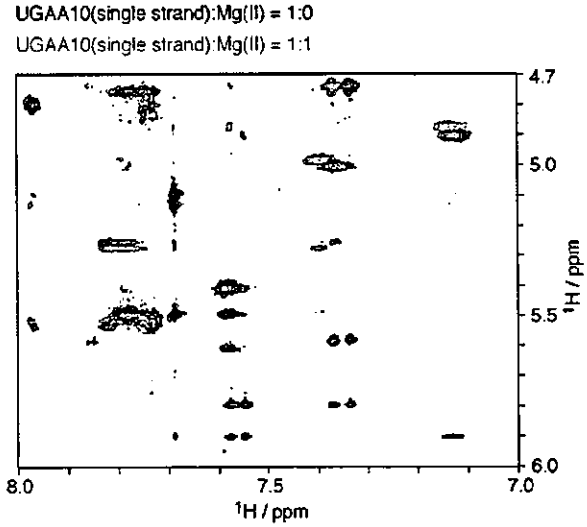

Figure 6. 2D ^{1}H–^{1}H NOESY spectra of UGAA10. Black spectrum: 2 mM UGAA10(single strand) without $MgCl_2$ (UGAA10(single strand): $MgCl_2$ = 1:0 mol/mol). Red spectrum: 2.0 mM UGAA10(single strand) with 2.0 mM $MgCl_2$ (UGAA10(single strand): $MgCl_2$ = 1:1). Spectra were recorded on Bruker DMX500 at 300 K; 4096*2048 complex points for a spectral width of 4006*4006 Hz.

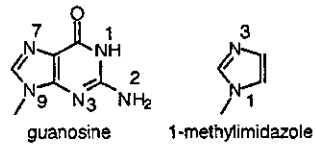

Figure 7. Chemical structures of guanine and 1-methylimidazole with numbering systems.

Lewis acid, Cd(II), in DMSO. Accordingly, the higher field shift (approximately 20 ppm) of the N7 resonance of the guanosine–Hg(II) or –Zn(II) in DMSO[28,29] is thought to be due to a direct coordination of guanosine to Hg(II) and Zn(II), since these metal ions belong to soft Lewis acids. In analogy, the higher field shift (19.6 ppm) of the N7(G7) in GA10 (Table 2)[5] indicates that the G7 residue directly coordinates to Cd(II) through N7. The lack of *J*-coupling between ^{113}Cd(II) and ^{15}N7(G7) is likely due to the fast exchange of the association–dissociation process of the Cd(II) binding to N7(G7).

On the other hand, in the cases for β-lactamase–Cd(II)[35] and ethylenediaminetetraacetic acid (EDTA)–Cd(II)[36] systems, *J*-coupling between ^{113}Cd and ^{15}N ($^1J_{N-Cd}$) were observed with only a slight chemical shift perturbation (Table 2). Although metalation sites of β-lactamase are imidazole rings of histidines and several imidazole rings surely coordinated to Cd(II), metalation did not affect ^{15}N chemical shifts of imidazole rings very much. This is quite different from Cd(II)–GA10 and Hg(II)–guanosine systems (no detectable $^1J_{N-M(II)}$ and large chemical shift perturbations). Unfortunately, we could not conclude the origins of the discrepancies at this moment. However, it was found that there are at least two patterns of appearance for ^{15}N NMR spectra which indicate an inner-sphere coordination of nitrogen to Cd(II). Therefore, caution must be

(33) Alei, M., Jr.; Morgan, L. O.; Wageman, W. E. *Inorg. Chem.* **1981**, *20*, 940–942.
(34) (a) Wakisaka, A.; Watanabe, Y. *J. Phys. Chem. B* **2002**, *106*, 899–901. (b) Mochizuki, S.; Wakisaka, A. *J. Phys. Chem. A* **2002**, *106*, 5095–5100.
(35) Damblon, C.; Prosperi, C.; Lian, L. Y.; Barsukov, I.; Soto, R. P.; Galleni, M.; Frere, J. M.; Roberts, G. C. K. *J. Am. Chem. Soc.* **1999**, *121*, 11575–11576.
(36) Hagen, R.; Warren, J. P.; Hunter, D. H.; Robarts, J. D. *J. Am. Chem. Soc.* **1973**, *95*, 5712–5716.

taken for the interpretation of ^{15}N NMR data when we determine the sort of chemical bonds from ^{15}N NMR data. For more definitive results, solid-state NMR with crystal powder of Cd(II)−guanosine complex might provide the definitive answer for the chemical bond formed between Cd(II) and N7 of guanosine, since in the crystal lattice association−dissociation dynamics is suppressed. In such a system, the Cd(II)−N7(G) bond can be determined by crystallography, and intrinsic *J*-coupling between $^{113}Cd(II)-^{15}N7(G)$ can be derived from solid-state NMR, and then ^{15}N and ^{13}C chemical shifts can be confirmed as well.

Roles of the Metal Ion at the A9/G10.1 Site. We have demonstrated that the altered motif in UGAA10, with an adenosine residue instead of a guanosine, was not sufficient to capture divalent cations from 2D $^1H-^1H$ NOESY spectra of UGAA10 (Figure 6). We had shown that nonspecific binding of metal ions was observed in the titration curves of GA10 at "mM" order, as well.[5] Thus, the altered motif is no longer thought to be a metal ion-binding motif. Interestingly, Sigel et al. indicated that N7 of adenosine is a much less efficient acceptor of metal ions than that of guanosine by means of potentiometric titrations at the nucleoside level.[37] They also demonstrated that basicities of nitrogen atoms were well-correlated with affinities of the nitrogen atoms to divalent cations, i.e., the order of affinities of N7 to divalent cations is guanosine > adenosine and the order of the basicities of N7 is guanosine > adenosine.[37] Therefore, we think that this effect is one of the major reasons for the reduced affinity of the altered motif to Mg(II). For more detailed physicochemical characterizations of this altered motif, titration experiments with $Co(NH_3)_6$(III) and Cd(II) are also required.

From the aspect of the roles of metal ions at the A9/G10.1 site, the above titration data of UGAA10 indicate a more important thing. Kinetic data by Ruffner et al. indicated that hammerhead ribozymes with the A10.1−U11.1 base pair (the altered motif) still possess 30% catalytic activities relative to those with the common sequence which includes the G10.1−C11.1 base pair.[7] Furthermore, in the sequence of the wild-type hammerhead ribozyme from the newt, A10.1−U11.1 is included instead of a G10.1−C11.1.[38] These data indicate that G10.1−C11.1 is not a strict requirement for the reaction catalyzed by hammerhead ribozymes, and G10.1−C11.1 can be replaced with A10.1−U11.1 without a loss of functions, although this base pair substitution significantly reduces a metal ion-binding ability of the motif (Figure 6). Therefore, if we assume that the metal ion at the A9/G10.1 site is a catalytic metal, reduced (almost loss of) metal ion-binding ability of UGAA10 is inconsistent with this assumption. Accordingly, it was suggested that the metal ion at the A9/G10.1 site is not a catalytic metal, although there might be a possibility that other conserved sequences might support metal ion binding to the altered motif upon conformational changes. Eckstein's group and Lilley's group indicated that hammerhead ribozymes changed their conformation in a divalent cation concentration-dependent manner.[9] The metal ion at the A9/G10.1 motif might be one of the structural cofactors for the formation of the γ-shape of hammerhead ribozymes.

(37) Kapinos, L. E.; Holy, A.; Günter, J.; Sigel, H. *Inorg. Chem.* **2001**, *40*, 2500−2508.
(38) (a) Forster, A. C.; Symons, R. H. *Cell* **1987**, *50*, 9−16. (b) Pabon-Pena, L. M.; Zhang, Y.; Epstein, L. M. *Mol. Cell Biol.* **1991**, *11*, 6109−6115.

Experimental Section

Sample Preparations. RNA oligomers were chemically synthesized, purified, and quantitated as described previously.[5,39] Synthesized RNA oligomers are the following:

GA10:r(GGACGAGUCC)

UGAA10:r(GGAUGAAUCC)

The basal solutions for NMR measurements contained 40 mM $NaClO_4$ and various concentrations of metal salts ($CdCl_2$, $Co(NH_3)_6Cl_3$, $MnCl_2$, and $NaClO_4$). To avoid precipitation of the metal−buffer complex and the resulting pH changes, no buffer was added to the solution used in the NMR measurements.[4,5,39] Instead, the pH of each solution was adjusted to 6 with the direct titration as described previously.[4,5,39] All titration experiments were performed at 313 K, unless stated in legends to the figures. Other spectral parameters are presented in legends to the figures.

Fluorescence Spectroscopy. We measured fluorescence spectroscopy using Tb(III) and Eu(III) as fluorescence probes. It is expected that fluorescence-detected circular dichroism (FDCD) can be observed if the above ions are recognized by the motif via an inner-sphere coordination, since a chirality is generated around a fluorescent metal center in such a case. In the GA10−Tb(III) system, a canonical-sensitized emission was observed (data not shown), and we found that Tb(III) was able to bind to GA10. However, a sensitized emission was not observed for the GA10−Eu(III) system (data not shown). Unfortunately, in such a case, the sensitized emission of Tb(III) might be arisen from a weak dipole−dipole (through-space) interaction,[40] which means that energy transfer can occur even if a nucleobase does not coordinate to Tb(III). Therefore, we could not get critical evidence for an inner-sphere coordination of metal ions to the motif (the A9/G10.1 site) from fluorescence spectroscopy and stopped further experiments with fluorescence spectroscopy, although the sensitized emission from the GA10−Tb(III) complexes is still interesting. Solution conditions for fluorescence spectroscopy were 1 μM GA10, 50 mM PIPES pH 6.5, 50 mM NaCl, and various concentrations (0.6, 2.6, and 4.6 μM) of $TbCl_3$ and $EuCl_3$. Spectra were recorded on a JASCO spectrofluorometer FP-750.

Acknowledgment. We thank Dr. Kodama at BERI, Osaka, for the critical discussion of fluorescence spectroscopy. Y.T. was supported by a Grant-in-Aid for Young Scientists (B) (15750136) and by a Grant-in-Aid for Scientific Research on Priority Areas (15025211) from the Ministry of Education, Culture, Sports, Science and Technology, Japan.

JA036826T

(39) Kasai, Y.; Tanaka, Y.; Morita, E. H.; Tanaka, Y.; Taira, K. *Nucleic Acids Res.* **2001**, (Suppl. 1), 81−82.
(40) Horrocks, W. D., Jr. *Methods Enzymol.* **1993**, *226*, 495−538.
(41) (a) Heus, H. A.; Pardi, A. *Science* **1991**, *253*, 191−194. (b) Katahira, M.; Kanagawa, M.; Sato, H.; Uesugi, S.; Fujii, S.; Kohno, T.; Maeda, T. *Nucleic Acids Res.* **1994**, *22*, 2752−2759.
(42) Jia, X.; Zon, G.; Marzilli, L. G. *Inorg. Chem.* **1991**, *30*, 228−239.
(43) Mukundan, S., Jr.; Xu, Y.; Zon, G.; Marzilli, L. G. *J. Am. Chem. Soc.* **1991**, *113*, 3021−3027.
(44) (a) Sherman, S. E.; Gibson, D.; Wang, A. H.-J.; Lippard, S. J. *Science* **1985**, *230*, 412−417. (b) Sherman, S. E.; Lippard, S. J. *Chem. Rev.* **1987**, *87*, 1153−1181. (c) Sundquist, W. I.; Lippard, S. J. *Coord. Chem. Rev.* **1990**, *100*, 293−322.

THE JOURNAL OF BIOLOGICAL CHEMISTRY
Vol. 279, No. 6, Issue of February 6, pp. 4760–4767, 2004
Printed in U.S.A.

Structure of the Ubiquitin-interacting Motif of S5a Bound to the Ubiquitin-like Domain of HR23B*

Received for publication, August 26, 2003, and in revised form, October 6, 2003
Published, JBC Papers in Press, October 29, 2003, DOI 10.1074/jbc.M309448200

Kenichiro Fujiwara‡, Takeshi Tenno‡§, Kaoru Sugasawa¶, Jun-Goo Jee‡‖, Izuru Ohki, Chojiro Kojima‡‡, Hidehito Tochio‡, Hidekazu Hiroaki‡, Fumio Hanaoka¶§§, and Masahiro Shirakawa‡¶¶**

*From the ‡Graduate School of Integrated Science, Yokohama City University, 1-7-29 Suehiro, Tsurumi, Yokohama, Kanagawa 230-0045, the §Graduate School of Science and Engineering, Ehime University, 3 Bunkyo, Matsuyama, Ehime 790-8577, the ¶Cellular Physiology Laboratory, Discovery Research Institute, RIKEN, 2-1 Hirosawa, Wako, Saitama 351-0198, the ‖Genomic Sciences Center, RIKEN, 1-7-22 Suehiro, Tsurumi, Yokohama, Kanagawa 230-0045, the **Department of Structural Biology, Biomolecular Engineering Research Institute, 6-2-3 Furuedai, Suita, Osaka 565-0874, the ‡‡Graduate School of Biological Sciences, Nara Institute of Science and Technology, 8916-5 Takayama, Ikoma, Nara 630-0101, and the §§Graduate School of Frontier Biosciences, Osaka University, 1-3 Yamada-oka, Suita, Osaka 565-0871, Japan*

Ubiquitination, a modification in which single or multiple ubiquitin molecules are attached to a protein, serves signaling functions that control several cellular processes. The ubiquitination signal is recognized by downstream effectors, many of which carry a ubiquitin-interacting motif (UIM). Such interactions can be modulated by regulators carrying a ubiquitin-like (UbL) domain, which binds UIM by mimicking ubiquitination. Of them, HR23B regulates the proteasomal targeting of ubiquitinated substrates, DNA repair factors, and other proteins. Here we report the structure of the UIM of the proteasome subunit S5a bound to the UbL domain of HR23B. The UbL domain presents one hydrophobic and two polar contact sites for interaction with UIM. The residues in these contact sites are well conserved in ubiquitin, but ubiquitin also presents a histidine at the interface. The pH-dependent protonation of this residue interferes with the access of ubiquitin to the UIM and the ubiquitin-associated domain (UBA), and its mutation to a smaller residue increases the affinity of ubiquitin for UIM.

Chains or single molecules of ubiquitin can be attached to cellular proteins, giving rise to poly- or monoubiquitination, respectively, which mediates distinct cellular signals (1–3). Polyubiquitination mainly targets proteins for degradation by the proteasome and can modulate diverse biological processes, such as cell cycle progression, apoptosis, antigen presentation, and stress response; by contrast, (monoubiquitination can act as both a endocytic sorting signal in vesicular transport and a key regulator of transcription, replication, and DNA repair (1–5). The versatility of ubiquitination signals is mediated by different downstream regulatory factors, many of which carry a UIM,[1] a ubiquitin-associated domain (UBA), or both (6–8). UIM was first identified in the proteasome subunit S5a and occurs in many proteins involved in rapid protein degradation or protein trafficking, such as endocytosis (Fig. 1*b*) (7).

So far, 27 UIM-containing proteins have been identified in humans (9). The S5a UIM requires a string of at least four Lys^{48}-linked ubiquitins for efficient binding (10). S5a of higher eukaryotes has two UIMs, located near each other in the C terminus. The C-terminal UIM by itself binds polyubiquitin chains as efficiently as the full-length S5a protein, whereas the N-terminal UIM alone binds polyubiquitin chains less efficiently (10). Nevertheless, a sequence alignment by Young *et al.* (10) revealed that S5a of *Saccharomyces cerevisiae* (Rpn10p) has only one UIM sequence that corresponds to the N-terminal UIM of higher eukaryotes (Fig. 1*b*). Recently, it has been shown that *S. cerevisiae* S5a contributes to the targeting of a subset of ubiquitinated substrates to the proteasome, but it is not the sole factor involved in polyubiquitin recognition (11, 12). Subunit S6′ of mammalian proteasome was also shown to recognize the polyubiquitin degradation signal (13). In contrast to S5a UIMs, those of the endocytic factors Hrs, Eps15, Eps15R, and Vps27 are proposed to bind monoubiquitin tags (8, 14, 15). The affinity between these UIMs and monoubiquitin seems low; the dissociation constant (K_d) for Hrs binding to monoubiquitin is 230–300 μM (16, 17).

Interactions of ubiquitin tags with UIM or UBA of downstream effectors are modulated by proteins that bear UbL domains, some of which are thought to bind UIM by mimicking ubiquitination. Similar to ubiquitin-like modifier proteins such as NEDD8, UbL domains share high sequence homology with ubiquitin (typically 24–33%) and thus adopt ubiquitin folds, as shown by the structure determination of the UbLs of PLIC-2, Parkin, and HR23B (18–20, 30).

Of the UbL-containing proteins, HR23B is the best characterized and has been shown to target the excision repair factor XPC/Rad4 and the endoplasmic reticulum-associated deglycosylation enzyme Png1p to the proteasome through interaction of its UbL with the proteasome (21–26). More recently, Rad23 (the *S. cerevisiae* homolog of HR23B) was proposed to deliver a variety of ubiquitinated cellular proteins to proteasome (27).

* This work was supported by grants from the Japanese Ministry of Education, Science, Sports and Culture (to M. S. and H. T.). The costs of publication of this article were defrayed in part by the payment of page charges. This article must therefore be hereby marked "*advertisement*" in accordance with 18 U.S.C. Section 1734 solely to indicate this fact.

The atomic coordinates and structure factors (code 1UEL) have been deposited in the Protein Data Bank, Research Collaboratory for Structural Bioinformatics, Rutgers University, New Brunswick, NJ (http://www.rcsb.org/).

¶¶ To whom correspondence should be addressed. Tel.: 81-45-508-7213; Fax: 81-45-508-7361; E-mail: shirakawa@tsurumi.yokohama-cu.ac.jp.

[1] The abbreviations used are: UIM, ubiquitin-interacting motif; UbL, ubiquitin like; HR23B, human homolog of RAD23 B; UBA, ubiquitin-associated domain; NOE, nuclear Overhauser effect; NOESY, NOE spectroscopy; GST, glutathione *S*-transferase.

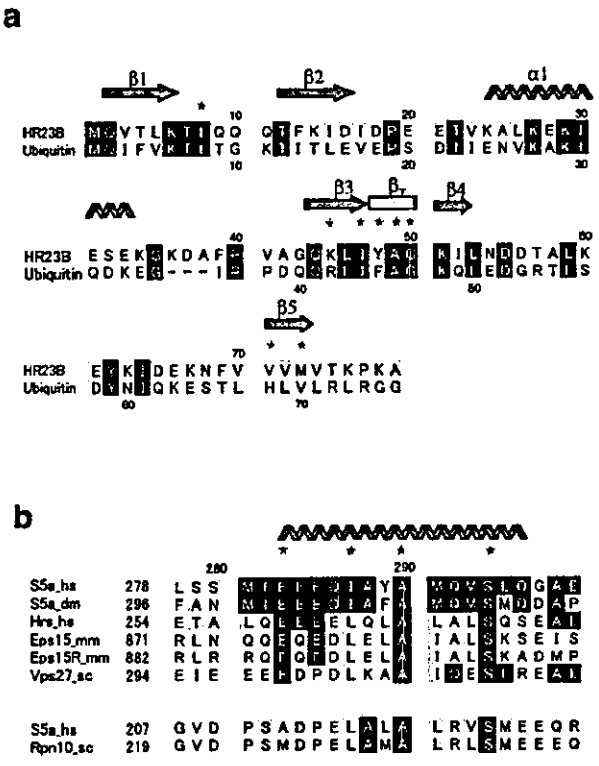

FIG. 1. **Sequence alignment of UbL and UIM.** *a*, sequences of human HR23B UbL and human ubiquitin. *b*, sequence alignment of the C-terminal UIM of human proteasome subunit S5a with UIMs of endocytic factors that have been either shown or implied to bind a ubiquitin tag (*top panel*) and of the N-terminal UIMs of human and *S. cerevisiae* S5a (Rpn10p) (*bottom panel*). The sequences are from human (*hs*), mouse (*mm*), *Drosophila melanogaster* (*dm*), and *S. cerevisiae* (*sc*). In *a* and *b*, identical residues are highlighted in *black*, and homologous residues are highlighted in *gray*. Secondary structural elements of HR23B UbL and S5a UIM are indicated. The residues shown to be important for the complex formation through structural or mutational analyses are marked with *asterisks*.

The interaction between the proteasome and the UbL domain of HR23B is essential for all of these functions. In higher eukaryotes, the C-terminal UIM of S5a has been proposed to be the receptor site for the UbL domain, to which it binds efficiently and with high affinity (K_d = 3.4 μM; this study, see "Results" and "Discussion"); by contrast, the N-terminal UIM does not bind to UbL (22). In yeast, however, S5a does not have a sequence corresponding to this C-terminal UIM (10) and does not bind to Rad23 (11). Instead, the proteasome subunit Rpn1 serves as its receptor. These observations may suggest that the HR23B receptor sites in the proteasome differ between yeast and higher eukaryotes.

The interaction between ubiquitin/UbL and UIM has been studied by mutagenesis and NMR chemical shift perturbation experiments (10, 16, 18, 19, 28–30). These experiments all suggest that the conserved hydrophobic patch composed of the side chains of Leu^8, Ile^{44}, and Val^{70} of ubiquitin serves as the binding site for S5a UIM or the proteasome.

To understand the structural basis for this recognition, we have solved the structure of the C-terminal UIM of human proteasome subunit S5a in complex with the UbL domain of human HR23B by solution NMR. A comparison of the UIM binding surface of UbL with the corresponding region of ubiquitin, coupled with extensive mutagenesis studies, indicates that the residues forming these interfaces are well conserved between UbL and ubiquitin, except for His^{68} of ubiquitin. This residue can regulate the access of the UIM or UBA to ubiquitin in a pH-dependent manner. The present structural and mutational data enable us to revise the consensus sequence of UIM.

EXPERIMENTAL PROCEDURES

Preparation of Proteins and Peptides—We expressed the N-terminal 87 residues of human HR23B, referred to as UbL, and residues 263–307 of S5a, referred to as UIM, as His-tagged proteins in *Escherichia coli* BL21(DE3). Labeled proteins were obtained by growing *E. coli* in synthetic media containing $^{15}NH_4Cl$ and $^{15}NH_4Cl/^{13}C$-glucose, respectively, and were purified chromatographically. UbL has an extra IIII-HHHH sequence at its C terminus, whereas UIM has an extra GSH sequence at its N terminus after cleavage by thrombin. The UIM-UbL complex was formed by titrating UIM into UbL, using changes in the amide group resonances of UbL in the ^{15}N,^1H HSQC (heteronuclear single quantum correlation) spectrum to indicate 1:1 stoichiometry. The UIM-UbL complex was in slow exchange on the chemical shift timescale. Samples for NMR measurements typically comprised 1.0 mM UIM-UbL complex in 20 mM potassium phosphate buffer (pH 6.8) and 5 mM KCl. Various combination of isotopically labeled UIM-UbL complex were used to obtain chemical shift assignments and distance restraints.

NMR Spectroscopy—NMR spectra were acquired at 303 K using a Bruker DRX500 or DRX800 spectrometer. For assigning the ^1H, ^{15}N, and ^{13}C resonances, we carried out a series of three-dimensional triple-resonance experiments (31). The stereospecific assignment of the methyl groups of the leucines and valines was achieved using 15% fractionally ^{13}C-labeled protein. Distance restraints were derived from ^{15}N and ^{13}C resolved three- and four-dimensional NOESY experiments with a mixing time of 100 ms. Intermolecular restraints were derived from the four-dimensional $^{13}C,^{15}N$-edited NOESY spectrum of a complex formed from ^{13}C-labeled UbL and ^{15}N-labeled UIM with a mixing time of 150 ms and three-dimensional ^{13}C-filtered-^{13}C-edited NOESY spectra of a complex formed from one unlabeled component and one $^{13}C,^{15}N$-labeled component with a mixing time of 100 ms. For torsion angle (ϕ, ψ) restraints, the backbone vicinal coupling constants ($^3J_{HN,H\alpha}$) were determined by means of HNHA experiment (31) and a data base search procedure based on backbone chemical shifts, using the program TALOS (32). pH titration of the unique histidine of ubiquitin, His^{68}, was carried out by measuring one-dimensional heteronuclear multiple-bond $^1H,^{15}N$ correlation spectra of ^{15}N-labeled human ubiquitin at 303 K.

Structure Calculations—For structure determination of the UIM-UbL complex, 100 structures were initially calculated by a simulated annealing procedure in CNS (33) and further refined by AMBER 7 (34). All interproton distance restraints were derived from unambiguously assigned NOE cross-peaks. The upper limits of NOE restraints were calibrated according to their intensities using ARIA protocols. For the final steps of the calculations, the restraints were included for 25 slowly exchanging backbone amides (2.8–3.4 Å (N–O) and 1.8–2.4 Å (H–O)). In total, 1,630 meaningful NOE restraints (639 intraresidual, 372 sequential, 211 medium range, 305 intramolecular long range, and 103 intermolecular) and 50 dihedral angle restraints were used.

Refinement using AMBER 7 consisted of 20-ps molecular dynamics, followed by 1000 steps of energy minimization. To approximate solvent interaction, a generalized Born model was used (35). Force constants were 20 kcal mol^{-1} $Å^{-1}$ for distance restraints and 150 kcal mol^{-1} rad^{-2} for dihedral angle restraints. Of refined 100 structures, the best 20 structures were selected and analyzed using MOLMOL (36), AQUA, and PROCHECK-NMR (37) software. No NOE was violated by more than 0.3 Å, and no torsion restraint was violated by more than 4°. The hydrogen bond between UIM Ser^{294} and UbL Gly^{50} was assumed on the basis of both mutagenesis of UIM Ser^{294} and observation of the bond in 98 of the 100 calculated structures.

Mutational Analyses—Mutant constructs were prepared with the GeneEditor *in vitro* site-directed mutagenesis system (Promega). The binding of S5a UIM to ubiquitin, HR23B UbL, and their mutants was determined by surface plasmon resonance using a BIACORE-X instrument. The equilibrium binding affinity of GST-UIM or its mutant immobilized on a CM5 chip was analyzed by monitoring the change in response units as a function of ubiquitin, UbL, or their mutant concentrations ranging from 0.1 to 500 μM at a flow rate of 20 μl/min in buffer containing 10 mM HEPES, pH 7.4, 150 mM NaCl, 3 mM EDTA, and 0.005% Surfactant P20. The binding of the UBA of yeast Dsk2p to ubiquitin was determined in the same way using a BIACORE-X instrument. A GST fusion protein that contains Dsk2p residues 328–373 (38) was immobilized onto a CM5 chip.

The effect of mutations on the affinity of S5a UIM for tetraubiquitin was examined by a surface plasmon resonance-based competition as-

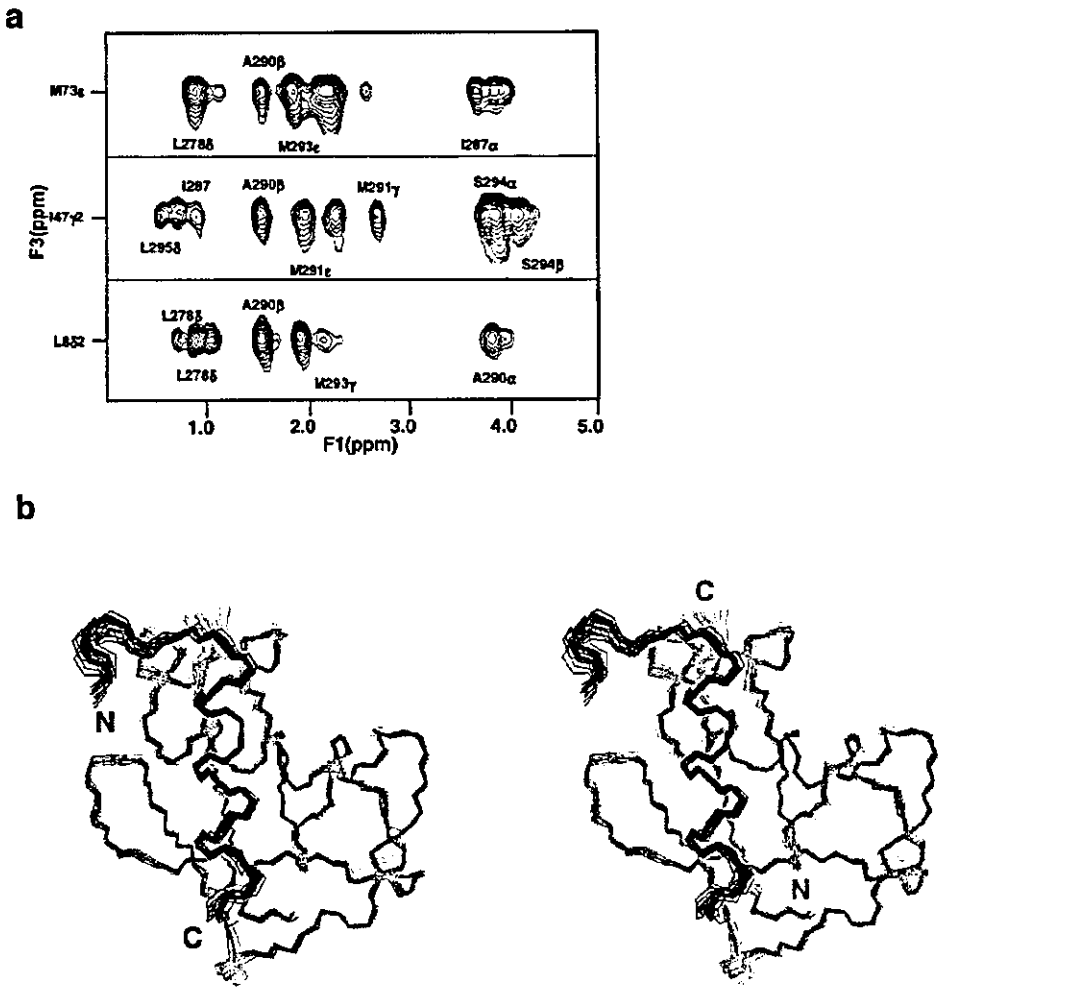

FIG. 2. **Structure determination of the UIM-UbL complex.** *a*, selected region of three-dimensional ^{13}C-filtered-^{13}C-edited NOESY spectra of a complex formed from $^{13}C,^{15}N$-labeled UbL and unlabeled UIM with a mixing time of 100 ms, depicting intermolecular NOEs. *b*, stereo view of the best fit superposition of the 20 final structures of the complex between UIM (*black*) and UbL (*blue*). Residues 263–277 and 297–307 of UIM are omitted from all figures for clarity.

say. The resonance curves were measured for 0.1 μM tetraubiquitin binding to immobilized GST-UIM in the presence of 40 μM His-tagged wild type UIM or its point mutants. A buffer containing 10 mM HEPES, pH 7.4, 150 mM NaCl, 3 mM EDTA, and 0.005% Surfactant P20 was used at flow rate of 20 μl/min. The effect of ubiquitin mutation of His^{68} to valine (H68V) for its binding affinity to the UIM of S5a was also analyzed by GST pull-down assay. 12 μg of GST-UIM was incubated with 3 μg of wild type or mutant ubiquitin in 100 μl of 20 mM HEPES (pH 7.9), 100 mM NaCl, 20% glycerol, 0.1% Nonidet P-40, and 200 μg/ml bovine serum albumin. The bound proteins were analyzed by GSH-mediated pull-down assay coupled with SDS-polyacrylamide gel electrophoresis and silver staining.

RESULTS

Structure Determination—The structure of the UIM of human proteasome subunit S5a in complex with the UbL domain of human HR23B was determined from a total of 1,730 NMR-derived restraints (Fig. 2*a* and Table I). The structure of residues 1–75 of UbL and that of the UIM residues 278–296 of S5a are well defined (Fig. 2*b*). By contrast, the terminal residues of UIM have no contact with UbL and are therefore disordered. In the complex, UbL folds into an α/β structure comprising a layer of five-stranded twisted β-sheet, backed by a long helix (Fig. 3*a*). It closely resembles the structures of ubiquitin (Ref. 39; Protein Data Bank code 1d3z), as indicated by the root mean square deviation of 0.741 Å over 30 Cα coordinates for residues in the regions of secondary structure elements. The UIM-bound UbL of HR23B has a structure similar to that of the unliganded form (30). Therefore, the UbL domain of human HR23B shares the same fold as members of the ubiquitin-like modifier family and other ubiquitin-like domains.

UIM adopts a hook-like conformation, consisting of an N-terminal loop (residues 278–282) followed by an α helix (residues 283–296), which are flanked on either side by N- and C-terminal unstructured regions (residues 263–277 and 297–307). The helix dominates the binding interface, fitting snugly along strands β3 and β5 of UbL, whereas the N-terminal loop runs alongside the loop that connects helix α1 and strand β3 of UbL, mediating minor interfacial contacts. The helical portion of the UbL-bound UIM of S5a, residues 284–296, adopts a nearly identical fold to the corresponding part of a free UIM of yeast Vps27p (residues 303–315), whose crystal structure was solved as an antiparallel four-helix bundle consisting of four molecules (40).

Recognition of UIM by UbL—UbL has three principle contact sites with the helix of UIM that mediate a central hydrophobic and two polar interactions. The hydrophobic contact site is defined by the outward facing residues Leu^8, Ile^{47}, Val^{71}, and

TABLE I
Experimental restraints and structural statistics of final 20 structures

Total number of distance restraints	1630
Intraresidue ($\|i - j\| = 0$)	639
Sequential ($\|i - j\| = 1$)	372
Medium range ($1 < \|i - j\| < 5$)	211
Intramolecular long range ($\|i - j\| \geq 5$)	305
Intermolecular	103
Number of hydrogen bonds	25
Number of dihedral angle restraints	50
Energies[a]	
Mean AMBER energy (kcal/mol)	−5172 ± 14
Mean van der Waals' energy (kcal/mol)	−937 ± 12
Mean constraint energy (kcal/mol)	18 ± 1
Mean deviations from ideal geometry	
Bond lengths (Å)	0.0100 ± 0.0001
Bond angles (°)	2.31 ± 0.01
Violation statistics	
Number of distance violation > 0.2 Å	0.6 ± 0.5
Maximum distance violation (Å)	0.27
Number of dihedral angle violation > 2°	0.3 ± 0.4
Maximum dihedral angle violation (°)	3.64
Root mean square deviation from the average structure[b]	
Backbone (Å)	0.34 ± 0.06
Heavy atoms (Å)	0.78 ± 0.06
PROCHECK statistics[b]	
Residues in most favoured regions (%)	91.4
Residues in allowed regions (%)	7.9
Residues in generously allowed regions (%)	0.6
Residues in disallowed regions (%)	0.1

[a] Generalized Born model of AMBER 7 was used.
[b] Residues 1–75 of HR23B and 278–296 of S5a were used.

Met^{73} of the UbL β-sheet; the side chains of these residues form a pocket that packs tightly around the methyl group of Ala^{290} of UIM (Fig. 3, *b* and *c*). Leu^{8} also forms hydrophobic interactions with Leu^{278} of UIM. Mutation of Leu^{8} or Val^{71} of UbL or of Ala^{290} of UIM largely abolishes binding, indicating that the surface complementarity of these residues is important for binding (Table II).

The association of the UIM helix is further stabilized by two polar interactions near both of its ends. Ser^{294} of UIM accepts a hydrogen bond from the main chain amide group of Gly^{50} of UbL, which adopts a consecutive type IV (residues 47–50) and type I′ (residues 48–51) β-turns (β_T; Fig. 3, *b* and *c*). This conformation, which is stabilized by an aromatic-methyl stacking interaction between the phenol ring of Tyr^{48} and the methyl group of Ala^{49}, places the amide group of Gly^{50} in a suitable position to form an intermolecular hydrogen bond. The significance of this bond can be seen by the total loss of binding that occurs when the hydroxyl group of Ser^{294} is replaced by a proton through a serine-to-alanine mutation (Table II).

The other polar interaction engages Glu^{283}, the N-terminal residue of the UIM helix, whose side chain carboxyl group can be in a position to make an electrostatic interaction with the side chain amino group of Lys-45 of UbL (Fig. 3*b*). Alanine substitution of Glu^{283} moderately decreases binding, suggesting that this charge complementarity is important for binding (Table II).

Comparison of UIM-binding Sites between UbL and Ubiquitin—Interestingly, all of the major UIM contact sites in UbL are conserved in ubiquitin. Residues Leu^{8}, Ile^{44}, Val^{70}, and His^{68} of ubiquitin create a hydrophobic surface that resembles the hydrophobic contact site on UbL (Fig. 3*d*). Previous mutational analyses have shown that, except for His^{68}, these ubiquitin residues are critical for proteasomal degradation and for binding to S5a and are essential for life in yeast (28, 41, 42).

The polar contact sites in UbL are also conserved in ubiquitin. The Phe^{45}-Ala^{46}-Gly^{47} segment of ubiquitin adopts a consecutive type IV (residues 44–47) and type I′ (residues 45–48) β-turns identical to that seen in the Tyr^{48}-Ala^{49}-Gly^{50} segment of UbL with an root mean square deviation of 0.12 Å across the main chain heavy atoms. Thus, the amide group of Gly^{47} of ubiquitin is in the same position as Gly^{50} of UbL, which forms a key hydrogen bond with Ser^{294} of UIM in the complex.

Finally, the positively charged side chain of Arg^{42} in ubiquitin is located in the same position as that of Lys^{45} of UbL and thus possibly mediates an electrostatic interaction with the conserved acidic residue at position 283 of UIM (Fig. 3*d*). Arg^{42} of ubiquitin has been shown to be essential for yeast viability (42).

The striking conservation of UIM-binding sites between ubiquitin and UbL suggests that the contact sites and mode of ubiquitin binding to UIM are similar to those observed in our structure. We confirmed that the effects of mutations in UIM are similar for UIM binding to UbL and UIM binding to tetraubiquitin; in other words, mutating Glu^{283}, Ala^{290}, or Ser^{294} in UIM impairs its binding to tetraubiquitin (Fig. 4). The importance of Ser^{294} of UIM was also shown by a previous mutagenesis study (10).

The Conserved UIM-binding Site of UbL and Ubiquitin—These shared features of the UIM-binding mode of UbL and ubiquitin raise the question of why UIM binds only weakly to monoubiquitin. The dissociation constant (K_d) defining the interaction between S5a UIM and monoubiquitin is 273 μM at pH 7 (Fig. 5*b*), and that between Hrs and monoubiquitin is 230–300 μM (16, 17). A detailed comparison of the surface of UbL and ubiquitin shows that the largest difference is a protrusion on ubiquitin caused by the bulky imidazole ring of His^{68} (Fig. 3*d*). This protrusion from the otherwise smooth ubiquitin surface may interfere with UIM binding, as can be seen in a structure of the S5a UIM-ubiquitin complex modeled by best fit superposition of the coordinates of ubiquitin to those of UbL in the lowest energy structure of the UIM-UbL complex; the imidazole of His^{68} encounters steric hindrance with the bound UIM (Fig. 3*d*). Consistent with this, substitution of the UbL residue at the same position, Val^{71}, with histidine impairs the ability of UbL to bind UIM (Table II).

To test whether the inability of monoubiquitin to bind S5a UIM is indeed due to steric hindrance, we replaced His^{68} of ubiquitin with valine, the amino acid that is found in this position in UbL and examined its effect on binding to UIM. This mutation increased the binding affinity, suggesting that the protrusion caused by His^{68} may inhibit the access of ubiquitin to UIM to some extent (Fig. 5*a*). This result suggests that the UIM-binding mode of ubiquitin is similar to that of UbL, consistent with the mutational data.

To determine whether His^{68} regulates ubiquitin binding, we examined the effect of protonation of its imidazole ring on the ability of ubiquitin to bind to UIM. The binding affinity correlated well with the pH-dependent protonation state of the His^{68} imidazole ring, as monitored by $H^{\delta 2}$ and $H^{\epsilon 1}$ chemical shifts (Fig. 5*b*). By contrast, this pH dependence was not observed for binding of the H68V mutant. Therefore, the His^{68} side chain probably has a regulatory role in the binding of ubiquitin to UIM.

We then examined whether this histidine of ubiquitin might regulate the binding of ubiquitin to UBA, another ubiquitin-binding motif that has been found in 79 human proteins (6, 9, 43). For this, we measured the binding affinity between ubiquitin and UBA from yeast Dsk2p at various pH values. It displayed a similar pH dependence to that between ubiquitin and UIM, suggesting that His^{68} of ubiquitin also regulates the binding of UBA to ubiquitin (Fig. 5*c*). This is consistent with recent structure determination of a CUE-ubiquitin complex (44). The CUE domain shows structure similarity with UBA domains and shares a common binding site on ubiquitin with UIM.

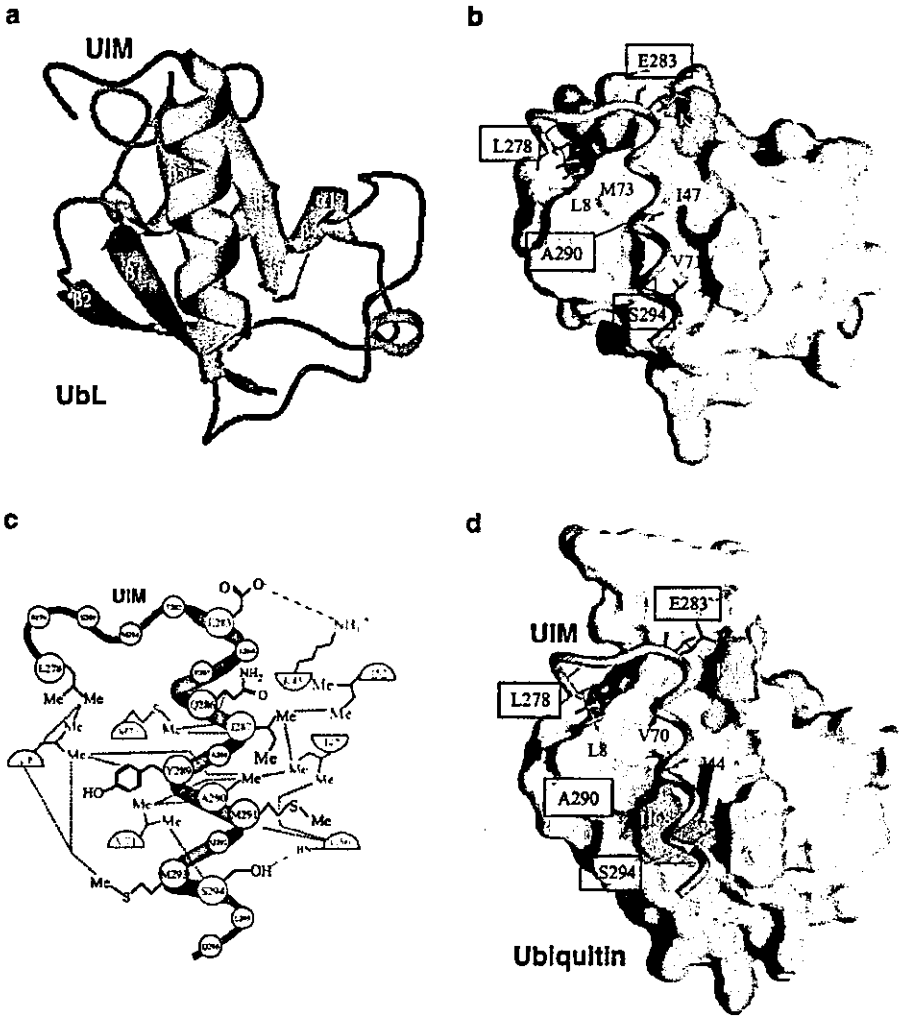

FIG. 3. **Structure of the UIM-UbL complex.** *a*, ribbon diagram of the lowest energy structure. UIM and UbL are colored *orange* and *blue*, respectively. Secondary structural elements of UbL are indicated. The Tyr^{48}-Ala^{49}-Gly^{50} segment of UbL, which forms β_T conformation, is shown in *green*. *b*, surface representation of the binding sites of UbL bound to UIM. Hydrophobic and charged residues are shown in *yellow* and *red*, respectively, and the β_T segment is shown in *green*. The side chains of UIM residues that interact with UbL are also shown. *c*, schematic diagram of the contacts between UIM and UbL. The main chain of UIM is shown in *red*. The side chains of UIM and UbL residues that form the interface are shown in *black* and *green*, respectively. Hydrophobic contacts are indicated by *blue dotted lines*, and hydrogen bonds and charged interactions are indicated by *red dashed lines*. *Me* denotes a methyl group. *d*, conserved UIM-binding sites in ubiquitin, deduced from the structure of the UIM-UbL complex, are shown on a model of the complex between human ubiquitin and UIM. Hydrophobic and charged residues are colored *yellow* and *red*, respectively, on the surface representation of human ubiquitin. The β_T segment, Phe^{45}-Ala^{46}-Gly^{47}, is shown in *green*. His^{68}, which causes the protrusion, is shown in *blue*. The model was constructed by best fit superposition of the coordinates of human ubiquitin (Protein Data Bank code 1d3z) to those of UbL in the lowest energy structure of the UIM-UbL complex.

DISCUSSION

UIM Interface of UbL—The UIM interface of UbL determined by our structure determination and mutagenesis studies is consistent with results from previous mutagenesis and chemical shift perturbation experiments of ubiquitin and UbLs (10, 16, 18, 19, 28, 29). All of those experiments suggest that the conserved hydrophobic patch composed of the side chains of Leu^8, Ile^{44}, and Val^{70} of ubiquitin is important for UIM or proteasome binding. The UIM-UbL complex reveals that the hydrophobic patch mainly functions as a pocket for the methyl group of Ala^{290}, which is conserved within UIM sequences (Fig. 1*b*) (7).

In addition to the contact mediated by the conserved hydrophobic patch, our complex structure shows that two polar interactions mediated by Glu^{283} and Ser^{294} of UIM contribute to the UIM-UbL association. Although the hydrogen bond through Ser^{294} is crucial for the binding, the electrostatic interaction between the side chains of Glu^{283} of UIM and Lys^{45} of UbL seems to be less important, because the substitution of Glu^{283} of UIM by alanine caused only a moderate effect in the binding of UIM to either UbL of HR23B or tetraubiquitin (Table II and Fig. 4). Notably, glutamic acid is well conserved at this position in UIM sequences that have been either shown or implied to bind a ubiquitin tags but not in the N-terminal UIM of human S5a or yeast S5a (Fig. 1*b*). Therefore, the weak interaction between human HR23B and the N-terminal UIM and that between yeast Rad23 and S5a may be attributed to the absence of glutamic acid at this position in their UIM sequences. Although the N-terminal UIM of human S5a binds to polyubiquitin chains much more weakly than does the C-